GDCh Review Angewandte
International Edition
www.angewandte.org
Check for updates

How to cite: Angew. Chem. Int. Ed. 2025, 64, e202511706
doi.org/10.1002/anie.202511706

Photo(electro)catalysis

Anisotropy of Single-Crystal Semiconductors in Photo(electro)Catalysis

Peng Cheng Ding, Yang Zhang, Wen Jing Li, Zheng Ming Li, Xue Lu Wang, Peng Fei Liu,* and Hua Gui Yang**

Abstract: Anisotropy in single-crystal semiconductors has emerged as a key design principle for understanding and advancing photo(electro)catalytic systems. The exposure of well-defined facets in single-crystal semiconductors introduces anisotropic variations in atomic coordination, electronic structure, and surface energetics, giving rise to directional charge transport and facet-specific reactivity. Such intrinsic differences coordinate the entire photocatalytic process, from charge excitation and separation to interfacial reaction kinetics. In this regard, effective utilization of anisotropy requires clarifying its impact on electronic structure, charge transport, and interfacial reactivity, along with its sensitivity to microenvironmental changes under realistic operando conditions. In this review article, we systematically examine the role of crystallographic anisotropy in light harvesting, charge carrier dynamics, and surface reactivity. We summarize recent advances in anisotropic material design, trace the evolution of the concept, and provide mechanistic insights based on experimental studies, theoretical models, and advanced characterization techniques. We further discuss current challenges and propose strategies to guide the rational application of anisotropy in catalyst design, aiming to expand its scope across a broader range of photo(electro)catalytic systems.

1. Introduction

Photo(electro)catalysis holds great promise for addressing global energy and environmental challenges through the direct conversion of solar energy into chemical fuels.[1,2] The design of efficient semiconductor materials is fundamental in the field of photo(electro)catalysis, which involves a sequence of interdependent processes including light absorption, charge carrier generation, and separation, along with surface redox reactions.[3,4] These steps are critical for driving complex, multi-carrier transformations such as water splitting,[5] carbon dioxide reduction,[6] and biomass conversion.[7] Among the materials investigated, single-crystal semiconductors have attracted particular interest due to their well-defined atomic structures, low defect concentrations, and the ability to expose specific crystal facets with tunable electronic and catalytic properties.[8]

Directional atomic arrangements in single-crystal semiconductors lead to facet-dependent anisotropy in physicochemical properties (Figure 1a). This anisotropy strongly affects photogenerated charge behavior and interfacial reaction kinetics.[9] Variations in surface energy, band-edge positions, and work function across facets induce internal electric fields that drive spatial charge separation. For example, single-crystal $SrTiO_3$: Al, characterized by its anisotropic crystal structure, demonstrates near-unity internal quantum efficiency for photocatalytic water splitting under illumination,[10] underscoring the decisive role of crystallographic anisotropy in enhancing charge separation and interfacial reactivity. Similar behavior has been observed in model material systems such as TiO_2[11] and $BiVO_4$[12] where facet-dependent properties critically dictate carrier dynamics and catalytic efficiency.

Therefore, mastering the principles of crystallographic anisotropy is essential for enabling the targeted design of advanced photocatalysts or photoelectrodes. Since our group initiated the selective exposure of the highly reactive {001} facets on TiO_2 by rational facet design,[13] there has been an increasing focus on the anisotropic nature of well-defined single-crystal systems across all stages of the photocatalytic process (Figure 1b).[14–17] Anisotropy fundamentally governs light-mattered interactions, charge dynamics, and interfacial reactivity. During light harvesting, orientation-dependent electronic band structures and optical selection rules, dictated by crystal symmetry, lead to anisotropic absorption and influence both the efficiency and spatial localization of electron-hole pair generation.[18,19] Within the bulk phase, directional variations in band alignment, surface energy, and

[*] P. C. Ding, Y. Zhang, W. J. Li, Z. M. Li, Prof. P. F. Liu, Prof. H. G. Yang
Key Laboratory for Ultrafine Materials of Ministry of Education, Shanghai Engineering Research Center of Hierarchical Nanomaterials, School of Materials Science and Engineering, East China University of Science and Technology, 130 Meilong Road, Shanghai 200237, China
E-mail: pfliu@ecust.edu.cn
hgyang@ecust.edu.cn

Prof. X. L. Wang
Physics Department & Shanghai Key Laboratory of Magnetic Resonance, School of Physics and Electronic Science, East China Normal University, Shanghai 200241, China
E-mail: xlwang@phy.ecnu.edu.cn

Prof. X. L. Wang
Institute of Magnetic Resonance and Molecular Imaging in Medicine, East China Normal University, Shanghai 200241, China

polarization effects give rise to anisotropic carrier transport, which in turn induces surface heterojunction and built-in electric field effects.[20] These internal fields act as endogenous driving forces that regulate the spatial separation of photogenerated charge carriers, thereby facilitating their directional migration and preferential accumulation on crystallographic faces that are both energetically and chemically favorable.[21] While on the surface, the preferential accumulation of charge carriers on distinct facets facilitates selective redox reactions, a process further modulated by facet-dependent adsorption behavior, surface reconstruction phenomena, and interactions with the surrounding liquid environment.[22,23] These conceptual advances have shifted the design paradigm from conventional isotropic optimization toward spatially resolved, anisotropy-guided strategies aimed at precisely controlling photocatalytic function.

Advances in synthetic techniques, such as facet-controlled crystal growth and site selective cocatalyst anchoring, have enabled the precise construction of anisotropic architectures. Meanwhile, recent developments in characterization methods have contributed equally,[27] with techniques such as surface photovoltage microscopy (SPVM),[25] Kelvin probe force microscopy (KPFM),[28] time-resolved photoemission electron microscopy (TR-PEEM),[25] single-particle photoluminescence (PL) spectroscopy,[29,30] and time resolved spectroscopy[31] offering spatial and temporal resolution of charge carrier dynamics on individual crystal surfaces. These advanced characterization techniques significantly deepen our understanding of the fundamental mechanisms underlying photocatalytic reaction processes (Figure 1b). Despite growing recognition of anisotropy as a key factor in promoting charge separation and enhancing facet-specific reactivity, several critical challenges still persist. These include uncovering its dynamic behavior under realistic reaction conditions, extending its relevance beyond a limited set of model systems, and formulating predictive principles that link anisotropic features to catalytic performance. Therefore, a focused and forward-looking assessment is both timely and necessary to guide future research in this emerging area.

In this review article, we examine the role of crystallographic anisotropy in single-crystal semiconductor-based photocatalysts or photoelectrodes, from fundamental principles to practical applications. We explore how anisotropy shapes light absorption, charge separation, and interfacial chemistry (Figure 2), and how these effects can be exploited through targeted material design. We also discuss emerging methods for visualizing and quantifying anisotropic behavior, and highlight key challenges and opportunities in this rapidly evolving field. We aim to advance the transition of photo(electro)catalysis from macroscopic asymmetric control toward microscale anisotropy-driven design, and provide a comprehensive perspective on anisotropy as a functional design element in next-generation photo(electro)catalysis techniques.

2. Anisotropy of Single-Crystal Semiconductors

2.1. Anisotropic Physicochemical Properties

Anisotropy refers to the directional dependence of a material's physicochemical properties, such as bandgap, optical

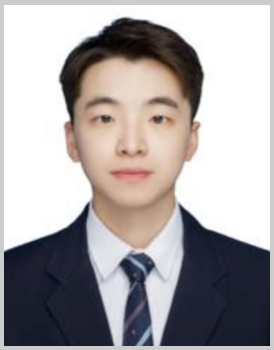

Peng Cheng Ding *received his B.E. degree from the Nanjing Tech University in 2023. He is currently a Ph.D. candidate under the supervision of Prof. Hua Gui Yang in School of Materials Science and Engineering at the East China University of Science and Technology. His current research interests are focused on the design of advanced catalysts for photocatalytic overall water splitting and the exploration of reaction mechanisms.*

Peng Fei Liu *received his B.S. and Ph.D. degrees from the East China University of Science and Technology (ECUST) in 2013 and 2018, respectively, and then worked in Prof. Hua Gui Yang's group as a Postdoctoral Research Fellow and an Associate Research Fellow. From 2023 to present, he worked as an Associate Professor at ECUST. His current research interests are focused on the design and synthesis of inorganic functional materials for (photo)electrocatalysis.*

Xue Lu Wang *received her Ph.D. degree from the East China University of Science and Technology in 2015, and then worked in Prof. Hua Gui Yang's group as a Postdoctoral Research Fellow. After finishing her postdoctoral training, she took a professor position at the East China Normal University in 2018. Her current research interests are focused on developing novel operando NMR technologies under controlled environments (atmosphere/light/electricity) to promote their innovative catalytic applications.*

Hua Gui Yang *received his Ph.D. degree from the National University of Singapore in 2005. He joined the University of Queensland in 2007 as a Postdoctoral Research Fellow. After finishing his postdoctoral training, he came back to China and took a professor position at the East China University of Science and Technology at the end of 2008. His main research interests are focused on the rational design and fabrication of functional materials for solar fuels.*

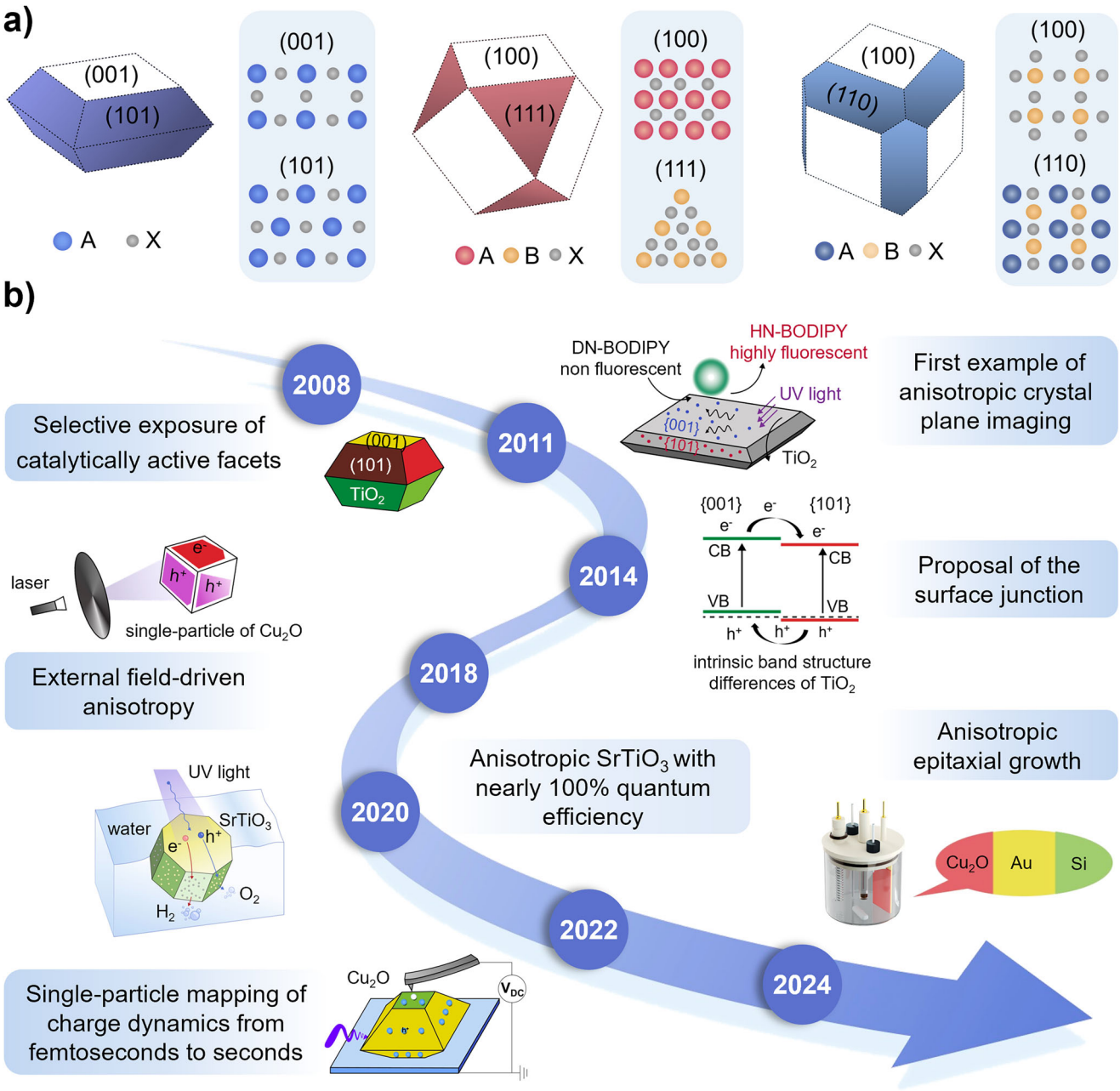

Figure 1. Schematic representations of geometrical shape and facet-dependent anisotropy (up), along with development progress and significant research achievements in semiconductor photo(electro)catalysts (down). a) Variations in atomic arrangement and coordination environment, which define the intrinsic properties of crystal facets and underpin the emergence of anisotropic physicochemical behavior. A, B, and X represent the atoms occupying the A-site, B-site, and X-site in the crystal structure, respectively. b) Key advances anisotropy of single-crystal semiconductors in photo(electro)catalysis: from material design and conceptual frameworks to the development of advanced characterization techniques. Copyright 2008, Nature Publishing Group.[13] Copyright 2011, American Chemical Society.[14] Copyright 2014, American Chemical Society.[17] Copyright 2018, Macmillan Publishers Limited, part of Springer Nature.[24] Copyright 2020, Spring Nature.[10] Copyright 2022, Spring Nature.[25] Copyright 2024, Spring Nature.[26]

absorption, and surface catalytic activity etc., across different crystallographic planes or axes.[32] In single-crystal semiconductors, particularly in the photo(electro)catalysis filed, anisotropy manifests in complex and diverse forms, which are closely associated with the intrinsic crystallographic structure. From a structural perspective, the crystals are classified into seven distinct systems based on their lattice symmetry, including cubic, hexagonal, and tetragonal systems. In the low-symmetry systems, such as hexagonal and tetragonal structures, these anisotropic properties are particularly pronounced, leading to significant direction-dependent variations in optical, electrical, and catalytic behaviors. However, even in the cubic systems, which appear macroscopically isotropic in terms of optics, intrinsic anisotropies persist at the electronic level, influencing band structure, and charge transport dynamics. For instance, on the (100) facet of a

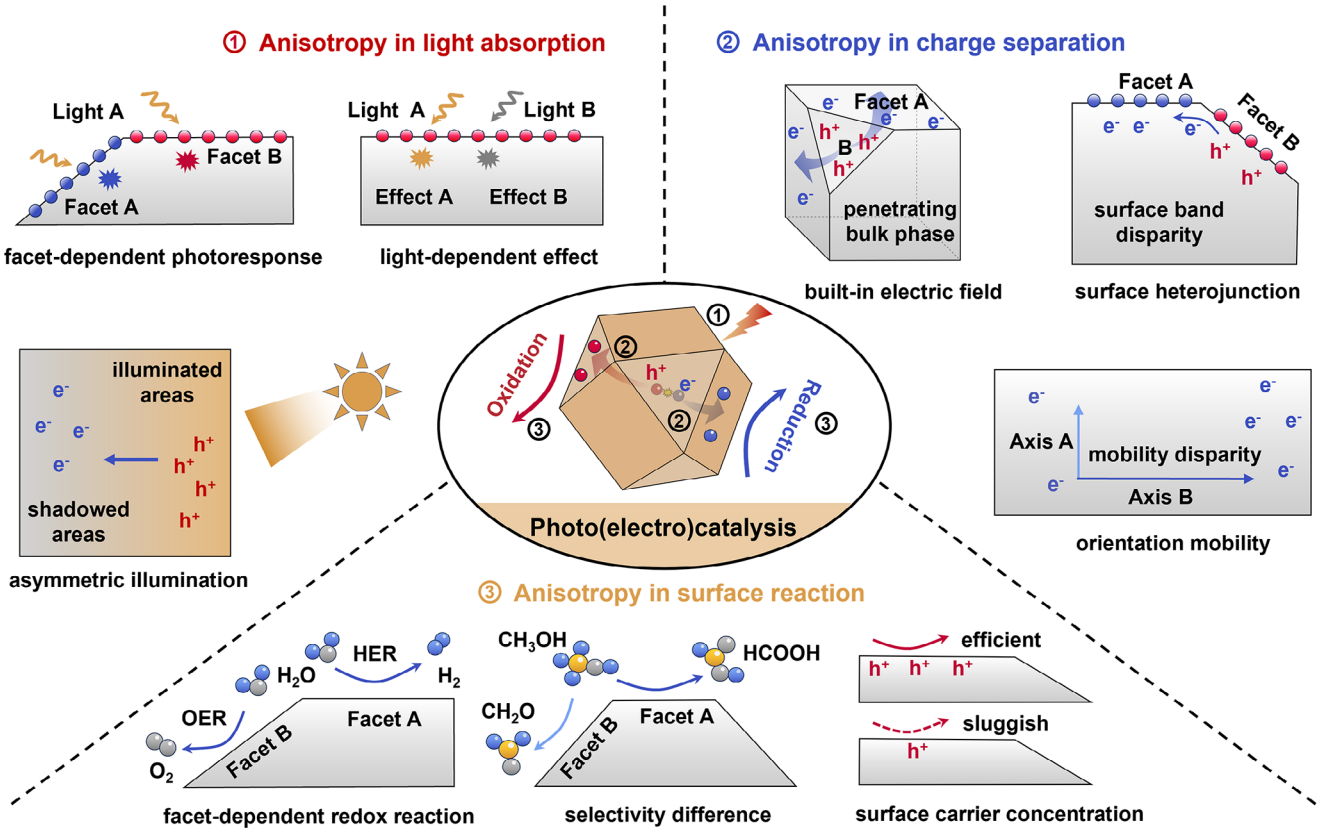

Figure 2. Schematic illustration of the anisotropy in photo(electro)catalysis. Schematic representation of facet-dependent photocatalytic redox reactions on anisotropic single-crystal semiconductors. The numbers indicate the key processes: (1) light absorption, (2) charge carrier separation and migration, and (3) surface redox reactions. Electron–hole representation: red spheres for electrons, blue spheres for holes (**center**). Anisotropic characterization of light source environment changes and crystal surface-specific response during the light absorption stage (**outer left**). Anisotropy phenomena in surface- and orientation-dependent carrier transport properties (**outer right**). Anisotropy in facet-dependent catalytic activity and selectivity across reaction stages (**outer bottom**). The deep blue, yellow, and dark gray spheres, represent H, C, and O atoms, respectively.

single high-symmetry $SrTiO_3$ nanocube, spatial separation of photogenerated charge carriers can also occur. Under low-intensity illumination, photogenerated holes tend to concentrate at the edges and corners of the cubic structure. In contrast, under high-intensity illumination, these charge carriers become more evenly distributed across the entire surface. This observation clearly demonstrates that, despite the inherently isotropic structure of cubic crystals, their internal physicochemical properties can exhibit pronounced spatial heterogeneity in response to external stimuli such as illumination conditions.[19] Therefore, anisotropic behavior is a prevalent feature of single-crystal semiconductors. To enable the rational design and development of high-performance single-crystal photocatalysts, it is crucial to explicitly identify and systematically harness these directional properties.

The anisotropic nature of single-crystal semiconductor photo(electro)catalysts is fundamentally rooted in the symmetry-breaking atomic architecture of their crystalline lattices, which propagates direction-dependent physicochemical properties from the bulk to the surface. In the bulk phase, the anisotropic arrangement of atoms dictates directional variations in bonding configurations, electronic band dispersion, and carrier effective mass, leading to crystallographic orientation-dependent charge transport and light–matter interactions. On the surfaces, the termination of lattice periodicity induces facet-specific coordination environments, where undercoordinated atoms undergo structural relaxation and electronic reconstruction. These processes create facet-dependent electronic states, modulate band edge positions, and establish localized surface energy landscapes that govern adsorption thermodynamics, defect formation, and catalytic site accessibility. Critically, the interplay between bulk-derived anisotropic carrier dynamics (e.g., directional electron-hole separation) and surface-driven facet selectivity (e.g., preferential adsorption of intermediates on high-energy facets) underpins the spatial heterogeneity of reactive sites and reaction kinetics. The intrinsic anisotropy at the atomic scale in crystalline materials provides a fundamental basis for modulating charge carrier dynamics and interfacial reactivity through rational structural design, thereby enabling a materials-based approach to enhance catalytic efficiency.

In addition to the intrinsic anisotropic characteristics of materials, their responses to external environments also exhibit distinct anisotropic features. Changes in factors such as incident light, mechanical strain, electric fields, and liquid-phase conditions can lead to heterogeneous responses both at the level of the entire crystal and across different crystallographic facets. While this increases the complexity

of optimizing and controlling crystal orientation for specific catalytic processes, it also presents promising opportunities for the rational design of reaction environments and catalytic devices.[33,34] The interplay between intrinsic anisotropic properties and external perturbations is particularly evident in photo(electro)catalysis, where optical responses are inherently facet-dependent due to variations in atomic composition and bandgap energies across crystal facets. This bandgap anisotropy directly influences the energy required for electronic transitions, leading to facet-selective differences in light absorption and subsequent charge carrier dynamics. In the model photocatalyst $SrTiO_3$, the penetration depth of incident light exhibits an exponential dependence on wavelength. At 310 nm, the light penetration depth is approximately 32 nm, while at 370 nm, it extends to 7.1 μm.[35] This difference in penetration depth further amplifies interfacial reaction disparities. For example, on the (110) facet of TiO_2 single crystals, the initial dissociation rate under 266 nm illumination is more than two orders of magnitude higher than that observed under 355 nm light.[18] Thus, the anisotropic characteristics of the crystal dynamically adapt to variations in external conditions. Strategically tuning environmental parameters to reinforce favorable anisotropic properties remains an intriguing avenue for further exploration.

2.2. Wulff Construction

The morphology and crystal configuration of single-crystal photo(electro)catalysts play a pivotal role in determining their physicochemical properties, thereby exerting a profound influence on their catalytic performance. Therefore, to effectively exploit the anisotropic physicochemical properties arising from tailored structural features, it is essential to rationally design the crystal morphology and exposed facets. From the perspective of material synthesis, the Gibbs–Curie–Wulff theory represents a classical and powerful theoretical approach for predicting the equilibrium morphology of crystals. This thermodynamic framework provides a direct link between intrinsic crystallographic anisotropy, controlled crystal growth, and facet-engineering strategies.[36]

The Wulff construction provides a fundamental thermodynamic principle for predicting the equilibrium morphology of crystals by minimizing the total surface free energy under isothermal and constant-volume conditions. Originally derived from Gibbs' formulation and mathematically formalized by Georg Wulff in the early 20th century,[37] this geometric model asserts that each crystallographic facet appears in proportion to its specific surface energy. As governed by the Wulff theorem, the linear growth rate of a specific crystallographic facet is directly proportional to its specific surface free energy:

$$\frac{\sigma_1}{r_1} = \frac{\sigma_2}{r_2} = \frac{\sigma_3}{r_3} = \cdots = \frac{\sigma_i}{r_i} \quad (1)$$

Where σ_i and r_i represent the specific surface free energy and center-to-facet distance of the i crystallographic plane, respectively.

Crystal facets with high surface energy and low interfacial tension typically grow at faster rates, often resulting in their minimal retention or complete disappearance as sharp edges or vertices. In contrast, facets with lower surface energy and higher interfacial tension grow more slowly and are more likely to be preserved in the final equilibrium morphology of the crystal. Clearly, in the rational design of key facets for anisotropic single-crystal semiconductor photo(electro)catalysts, the Wulff construction provides critical insights into the anisotropic nature of crystal growth.

Recent advances have significantly extended the classical Wulff theory into atomistic domains through first-principles calculations, enabling accurate surface energy predictions at the nanoscale.[38] This approach has been instrumental in enabling the facet-selective synthesis of semiconductors for photoelectrochemical (PEC) applications, where the controlled exposure of specific crystallographic planes, such as the reductive {100} and the oxidative {110} facets, enhances spatial charge separation and optimizes interfacial redox kinetics. In addition, kinetic extensions of the Wulff construction have been developed to account for supersaturation-driven growth dynamics and facet-specific growth rates, offering a more accurate description of the nonequilibrium morphologies commonly encountered under practical synthesis conditions.[39,40] These approaches bridge thermodynamic shape predictions with dynamic growth behavior, accounting for solvent effects, additives, and local concentration gradients.

However, several intrinsic limitations constrain the universal applicability of the Wulff construction. At the nanoscale, particle-size-dependent deviations often emerge due to atomic packing constraints and pronounced edge and vertex effects, resulting in morphological features that deviate from those predicted by continuum-based models.[36] Moreover, real crystal growth conditions frequently depart from equilibrium. Factors such as supersaturation, interfacial stress, and surfactant adsorption can kinetically stabilize high-energy facets that are thermodynamically unfavorable and therefore absent in ideal Wulff-predicted shapes.[41,42] In particular, for strongly polar or non-centrosymmetric crystals, intrinsic electric dipole moments or local dipolar interactions can induce asymmetric surface energies even among crystallographically equivalent facets, further complicating accurate morphological prediction via conventional Wulff constructions.[43] As a result, the experimentally observed morphologies of photocatalysts or photoelectrodes typically arise from a complex interplay between thermodynamic driving forces and kinetic modulations.

Despite these limitations, the Wulff construction remains a powerful conceptual and computational tool for rational catalyst design. Its integration with density functional theory (DFT), crystal orbital population analysis, and machine learning has opened new pathways for predicting morphology–reactivity relationships across diverse semiconductor systems.[44] Continuous improvements to the Wulff-based model, including particle size calibration, dynamic morphological evolution analysis, and in situ characterization techniques, have reinforced the importance of developing structure engineering in a systematic and predictive manner.

These advancements have laid the foundation for theory-driven strategies that can guide and expedite experimental progress.

2.3. Anisotropic Structure Engineering

Crystal morphology is governed by facet-specific surface energies, which influence atomic arrangements and electronic structures that ultimately determine catalytic behavior. As previously discussed, while thermodynamic principles favor the exposure of low-energy facets, achieving superior catalytic performance increasingly necessitates the deliberate engineering of high-energy surfaces to enhance charge separation and stabilize reactive intermediates.[13] To meet the intrinsic requirements of efficiency and selectivity in catalysis, anisotropic structural engineering offers a powerful strategy for directing charge transport through the spatial control of semiconductor crystal facets.[45] By precisely tuning facet exposure, this approach exploits inherent variations in atomic arrangements and electronic density of states across distinct crystallographic planes to construct oriented charge transport pathways. Prominent synthetic strategies include wet-chemistry methods,[13] molten salt synthesis,[10] and single-crystal thin-film techniques[26] et al., offering robust platforms for designing anisotropic single-crystal semiconductor materials tailored for photo(electro)catalysis.

Selective adsorption of organic molecules, inorganic ions, or their complexes as capping agents in wet-chemical synthesis enables precise modulation of crystal morphology.[46] By preferentially binding to specific crystallographic facets, these species reduce surface energies in a facet-dependent manner, thereby modulating the relative growth rates of different orientations and directing anisotropic crystal evolution.[47,48] This dynamic regulation of interfacial thermodynamics facilitates controlled exposure of targeted crystal planes, offering a versatile strategy for fabricating facet-engineered single-crystal semiconductors. The selectivity and adsorption affinity of capping agents are largely determined by the density of undercoordinated surface atoms. By tuning growth kinetics along defined crystallographic directions, it becomes possible to synthesize single crystals with programmable facet exposure ratios. As a representative example, our group theoretically analyzed the impact of 12 non-metallic elements on the surface free energy of different facets in anatase TiO_2 (Figure 3a,b). Density functional theory calculations predicted that fluoride adsorption could increase the proportion of the {001} facet to 47% (Figure 3c), enabling the successful synthesis of highly active {001}-facet-dominated single crystals.[13] This breakthrough overcame the constraints imposed by conventional thermodynamic equilibrium and represented an early example of theoretical predictions guiding experimental advancements. Building upon this, we developed a mixed capping strategy using citrate and HF to synthesize TiO_2 crystals with continuously varied Miller indices, resulting in curved surface architectures (Figure 3d). By adjusting the citrate concentration, we surpassed the limitations of classical Wulff construction and achieved uniform growth across multiple microfacets.[16]

To further extend facet engineering concepts, we recently developed a molten salt-assisted recrystallization strategy starting from hydrothermally synthesized low-crystalline $SrTiO_3$ precursors. Trace amounts of aliovalent Al^{3+} ions were introduced to selectively promote the exposure of high-energy {111} facets while preserving the presence of {100} planes, resulting in well-defined single crystals with tunable {100}/{111} facet ratios (Figure 4a,b).[49] In a subsequent study, we established a one-step molten salt synthesis strategy to establish a precise anisotropic facet engineering approach for $SrTiO_3$ single crystals, by systematically tuning the Al/Ti precursor ratio over a broad range (0.25–75 mol%) under molten salt conditions.[50] By introducing miscible $AlCl_3$ into a $SrCl_2$ molten flux, a controllable and homogeneous Al^{3+} environment was achieved. This enabled directional evolution from pure {100} facets to well-defined cuboctahedral ({100}/{111}) and ultimately {100}/{110}-dominated morphologies (Figure 4c). Compared to conventional solution-based and hydrothermal methods, molten salt synthesis offers unique advantages in fabricating highly crystalline, high-index-faceted, and morphology-controlled single-crystal catalysts. For instance, Wang and colleagues employed a LiCl/KCl molten salt medium, utilizing dicyandiamide (DCDA) as a precursor in a high-temperature salt-mixing reaction. This approach successfully yielded PTI/Li^+Cl^- single crystals featuring exposed {0001} basal planes and {1010} prismatic facets, effectively overcoming the crystallinity limitations of traditional polymeric carbon nitrides (PCNs).[52] Likewise, Liu et al. synthesized Sc-doped rutile TiO_2 single crystals with co-exposed (101) and (110) facets via molten salt synthesis, achieving well-defined surface terminations.[53] Collectively, these studies demonstrate that molten salt synthesis provides a robust platform for producing high-quality anisotropic single-crystal semiconductors with precise facet control, which is particularly advantageous for enhancing overall water splitting performance.[10,52,53] Despite these advances, molten salt strategies remain less explored than wet-chemical methods. Beyond practical challenges such as mass transport non-uniformity, morphology control, and size uniformity, several fundamental aspects remain unresolved. The general influence of different salt compositions on crystal growth mechanisms is not fully understood, nor is the role of additive ions in directing facet-selective growth. Furthermore, a universal theoretical framework and synthesis strategy for rationally exploiting molten salt media to obtain high-quality single crystals is still lacking. Addressing these gaps will be key to advancing both the precision and scalability of molten salt synthesis in semiconductor photocatalysis.

Beyond single-crystal particles, precise control over anisotropy is equally critical for the growth of single-crystalline photoelectrode thin films. Li et al. demonstrated a novel Voronoi oxygen sublattice matching mechanism, enabling the preferential growth of lattice-mismatched anisotropic single-crystal thin films on transparent conducting oxides (TCOs).[51] As illustrated in Figure 4d, a continuous interface was formed between the (110) facet of hexagonal α-Fe_2O_3 and the (101) facet of tetragonal FTO, owing to the high degree of geometric and topological matching in their oxygen sublattices. Through Voronoi decomposition based on

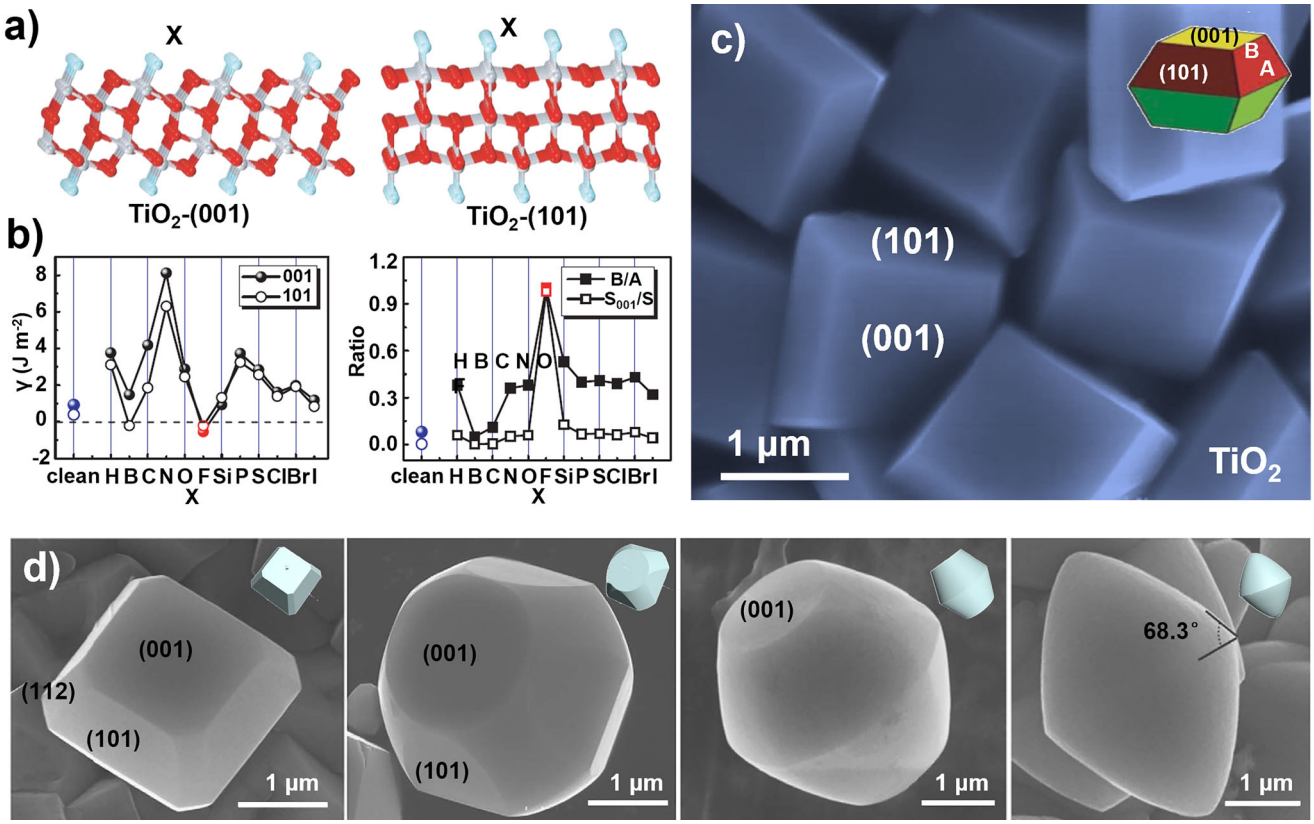

Figure 3. Structural engineering of anisotropic single-crystal photo(electro)catalysts via wet-chemical synthesis. a) Unrelaxed (001) and (101) surfaces surrounded by adsorbate X atoms. b) Calculated energies of the (001) and (101) surfaces surrounded by X atoms, plots of the optimized value of B/A and percentage of {001} facets for anatase single crystals with various adsorbate atoms X. c) SEM images of wet-chemical synthesis-based anatase TiO_2 single crystals. Copyright 2008, Nature Publishing Group.[13] d) SEM images and corresponding geometric models of anatase TiO_2 single crystals synthesized with different amounts of citrate. Copyright 2014, Macmillan Publishers Limited.[16]

the positions of interfacial oxygen atoms, local coordination environments between the overlayer and the substrate were effectively aligned. This strategy enables the construction of low-energy, cooperative interfaces even in systems with substantial lattice mismatch. Similarly, Pan et al. employed a liquid-phase epitaxy strategy using Au as a buffer layer to grow Cu_2O single-crystalline films on Si substrates despite a large lattice mismatch (~25.8%). Through coherent interface engineering based on the Au/Si eutectic, high-quality Cu_2O films with (100), (110), and (111) orientations were fabricated under ambient conditions, effectively integrating facet control into PEC-oriented film design.[26] In another example, $BiVO_4$ photoelectrodes with preferentially exposed (040) facets were synthesized via a seed-assisted hydrothermal route using PVP as a structure-directing agent, followed by electrochemical treatment to introduce oxygen vacancies and tune crystallographic orientation.[54]

Crystal facet engineering has emerged as a broadly applicable strategy for modulating charge separation efficiency and surface reactivity in photocatalytic systems. Originally developed for conventional metal-oxide semiconductors such as TiO_2, $SrTiO_3$,[55] and $BiVO_4$,[12] this approach has been successfully extended to emerging metal oxynitrides and oxysulfides (e.g., $ATaO_2N$,[56] where A=Sr, Ca, Ba; $Y_2T_2O_5S_2$[20]), as well as to nonmetallic semiconductors including graphitic carbon nitride (g-C_3N_4),[57] covalent organic frameworks (COFs),[58] and metal-organic frameworks (MOFs).[59] A central challenge lies in developing facet-selective capping agent systems that are tailored to the crystallographic and surface chemistry of each material class. Notably, the relationship between capping agent concentration and crystal facet exposure is often nonlinear: small variations in concentration can induce either abrupt transitions in facet dominance or continuous gradient changes in surface composition. This sensitivity introduces challenges for precise control, while simultaneously offering opportunities for multidimensional tuning of crystal morphology and function. In parallel, molten salt synthesis has enabled the fabrication of high-quality single-crystalline films with well-defined facets at scales exceeding 100 m^2, providing a promising platform for integrating facet-engineered materials into large-area solar energy conversion systems.[60] In addition, thin films grown via liquid-phase epitaxy or template-assisted methods have demonstrated not only precise crystallographic orientation control, but also excellent compatibility with scalable deposition techniques and device-level integration.[61] As numerous excellent reviews have comprehensively summarized the synthesis strategies for single-crystal materials in the context of crystal surface engineering, this discussion focuses on selected examples

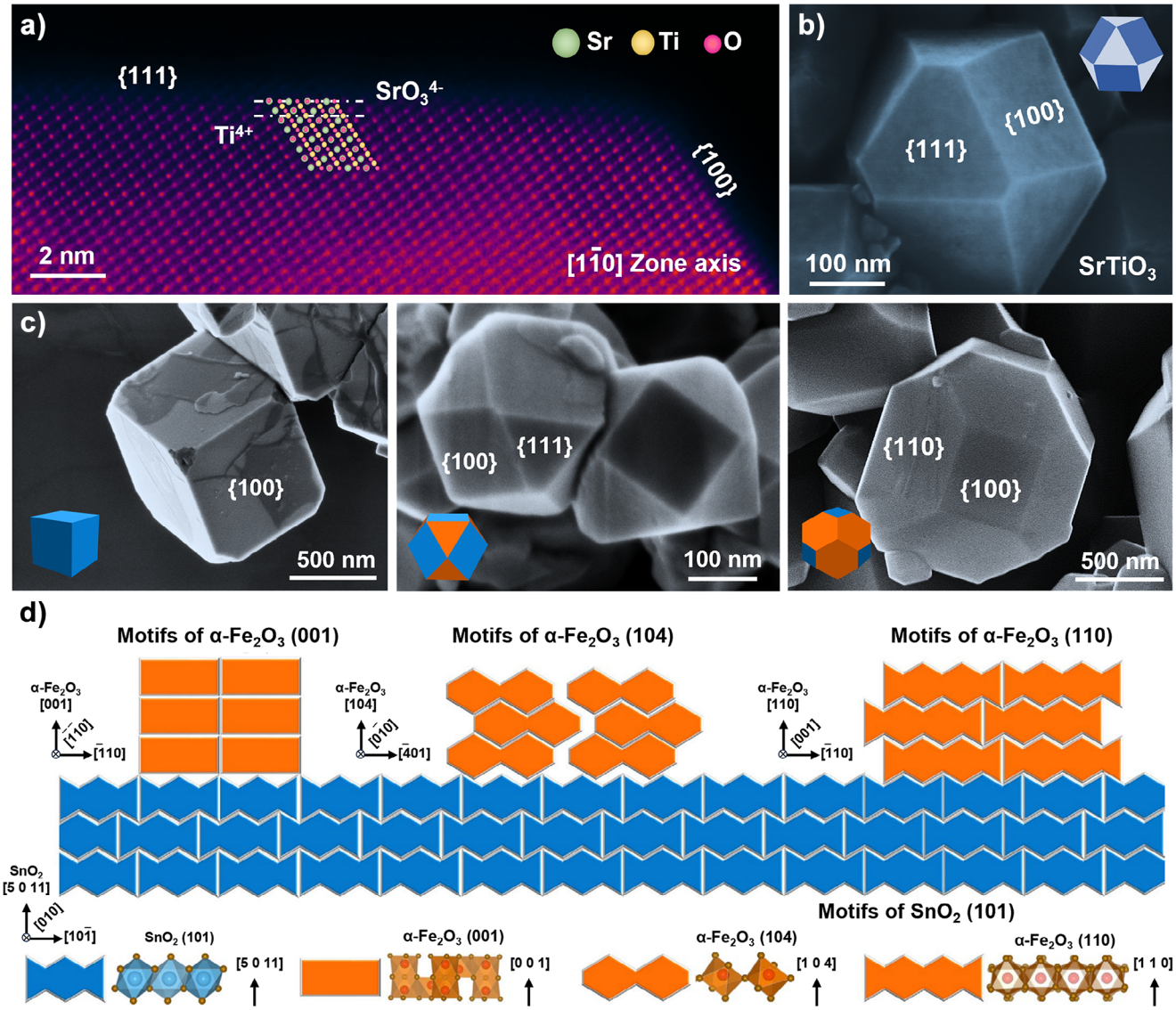

Figure 4. Molten salt synthesis of anisotropic single crystal photo(electro)catalysts and structural engineering of single-crystal thin-film photoelectrodes. a), b) Molten salt method-based crystal characterization of cuboctahedron $SrTiO_3$ single crystals. Copyright 2024, American Chemical Society.[49] c) SEM images of $SrTiO_3$ single crystals of cubic with {100} facets, truncated cube with {100} and {111} facets, edge-truncated cube with {100} and {110} facets. Copyright 2025, Wiley-VCH GmbH.[50] d) Woven films of α-Fe_2O_3 stacked at the subunit cell level on SnO_2 during growth (orange and blue patterns, respectively). Copyright 2024, Springer Nature.[51]

and omits detailed descriptions of the synthesis methods for conciseness.[62,63]

These new strategies for crystal structure design lay the groundwork for the mechanistic influence of anisotropy in photocatalysts and photoelectrode, where crystallographic orientation and atomic coordination dictate charge transport, light–matter interactions, and catalytic reactivity. Anisotropic effects extend across both bulk and surface properties, influencing carrier mobility, optical bandgaps, charge trapping, and interfacial kinetics. The intricate interplay among these factors necessitates a systematic approach to anisotropy engineering. In the following sections, we explore the role of anisotropy in light absorption, charge separation, transport, and surface catalytic reactions, offering a mechanistic perspective on how directional control at the atomic and mesoscale levels can unlock enhanced photo(electro)catalytic performance.

3. Anisotropy in Light Absorption

Photocatalytic reactions initiate with the absorption of light energy by a semiconductor photocatalyst, promoting electrons from the valence band to the conduction band and generating electron-hole pairs. This light-driven electronic excitation constitutes the essential first step toward converting photon energy into chemical energy.[64] Consequently, the efficiency of photon absorption directly determines the density and activity of charge carriers. In single-crystal

semiconductors, facet-dependent light absorption is governed by the specific variations in surface atomic configuration, coordination state, and localized electronic density.[65] As discussed in Section 2.1, different crystal facets exhibit varying sensitivities to light of the same wavelength, while light of different wavelengths interacts differently with the same crystal facet. This intricate interplay between the catalyst and incident light gives rise to an inherent anisotropic light absorption mechanism.

3.1. Intrinsic Anisotropic Absorption

Crystal facets exhibit strong sensitivity to incident light, with variations in exposed surfaces within a single catalyst crystal giving rise to distinct electronic structures. This results in facet-dependent surface bandgap variations, thereby altering the absorption edge and the range of effectively captured wavelengths.[66] Since the bandgap of a semiconductor directly determines the minimum energy threshold for light absorption, understanding and utilizing the anisotropic bandgap properties of different crystal facets has been a long-standing research focus. Early studies by Labat and colleagues employed various theoretical methods to simulate the low-index surfaces of TiO_2, revealing that differences in surface atomic coordination, electronic structure, and density of states contribute to facet-dependent bandgap variations. For instance, on the rutile (110) facet, an abundance of Ti^{3+} 3d states contributes to the lower portion of the conduction band, while O 2p states primarily shape the upper valence band. This electronic configuration influences transition characteristics, making the (110) facet more suitable for absorbing specific wavelengths of light. In contrast, the anatase (101) facet exhibits relatively minor variations in density of states, leading to more uniform absorption properties across different crystal planes. Notably, the bandgaps of the rutile (110) and anatase (101) facets were determined to be 3.96 and 4.63 eV, respectively, compared to their corresponding bulk bandgaps of 4.05 and 4.50 eV.[66] However, further experimental investigations into anatase TiO_2 with well-defined, cleanly exposed facets revealed intriguing bandgap differences. As shown in Figure 5a, facet-dependent anisotropic light absorption has been observed in anatase TiO_2 single crystals. Although the {001} facet has a higher density of undercoordinated Ti_{5c} atoms, it exhibits a redshifted absorption edge and a lower conduction band position compared to the {101} facet, leading to weaker reduction potential of photogenerated electrons. This counterintuitive behavior highlights the importance of facet-specific electronic structures, particularly band-edge alignment, in determining light-harvesting efficiency during the excitation stage. The observed shift is attributed to surface relaxation and electronic reconstruction on the {001} facet, which modulate the local density of states and band-edge positions. These results demonstrate that subtle variations in surface electronic structure can strongly influence the optical properties of single-crystal semiconductors.[15] In Ye's study, the evidence for facet-dependent anisotropic light absorption is even more enlightening. Diffuse reflectance spectroscopy revealed that compared to Ag_3PO_4 cubes with fully exposed {100} facets, rhombic dodecahedral Ag_3PO_4 with exposed {110} facets exhibited a redshift in the absorption edge of approximately 30 nm. This indicates that the {110} facet of Ag_3PO_4 absorbs longer wavelengths more effectively than the {100} facet, highlighting its superior light-harvesting capability.[68]

Beyond the intrinsic facet-dependent light absorption of single-crystal semiconductors, introducing heterostructures, defects, or dopants at specific facets can further enhance anisotropic optical responses. For example, the oxidation of surface Ti interstitials on {011}-exposed TiO_2 thin films led to the formation of a two-dimensional pure TiO_2 phase, red-shifting the absorption edge from 415 to 590 nm. By leveraging the anisotropic absorption properties of different TiO_2 phases, a metastable phase was engineered through surface structure modifications, enabling visible-light absorption (bandgap: 2.1 eV) in a pristine, dopant-free TiO_2 system.[69,70] Additionally, coupling metal nanoparticles (such as gold, silver, and copper) with anisotropic semiconductor structures can leverage localized surface plasmon resonance (LSPR) to induce collective oscillations of free electrons under illumination. This process generates a localized electric field enhancement, significantly improving the absorption of specific wavelengths by semiconductors or molecular materials. Unlike traditional semiconductors where the bandgap dictates the light absorption range, the LSPR effect enables strong absorption in the visible and even near-infrared regions by enhancing light absorption through localized surface plasmon resonance. Majima et al. demonstrated that anisotropic crystal facets facilitate electron injection from photoexcited Au NPs into the {001} facet of TiO_2, thereby enhancing photon absorption in the visible and infrared regions. Interestingly, the light absorption intensity exhibited differences when Au NPs were loaded onto different TiO_2 surfaces. Moreover, even when Au was deposited on the same facet, the structural characteristics of the TiO_2 substrate introduced variations in optical absorption.[71] Thus, leveraging the anisotropic light absorption properties of well-defined single-crystal semiconductor facets requires careful design considerations. The type of exposed facets, their relative proportions, and surface modifications all play critical roles in optimizing light absorption.

Variations in surface bandgap and band edge positions determine the absorption of photons with specific energies. However, given that photons from different spectral regions possess distinct energy levels, the reactivity differences induced by variations in photon energy when light of different wavelengths interacts with the same semiconductor facet are crucial considerations for refining photocatalytic models. For instance, Yang et al. demonstrated that the relative quantum yield of H_{BBO} from the photoinduced dissociation of CH_3OH on TiO_2(110) at 266 nm is over 100 times higher than that at 355 nm, indicating a strong wavelength dependence of the reaction. This finding challenges the conventional focus on charge carrier quantity while overlooking the impact of charge carrier energy.[18] However, due to the extensive number of experimental variables involved in the interaction of different light sources with anisotropic crystal facets, isolating the effect of charge carrier energy

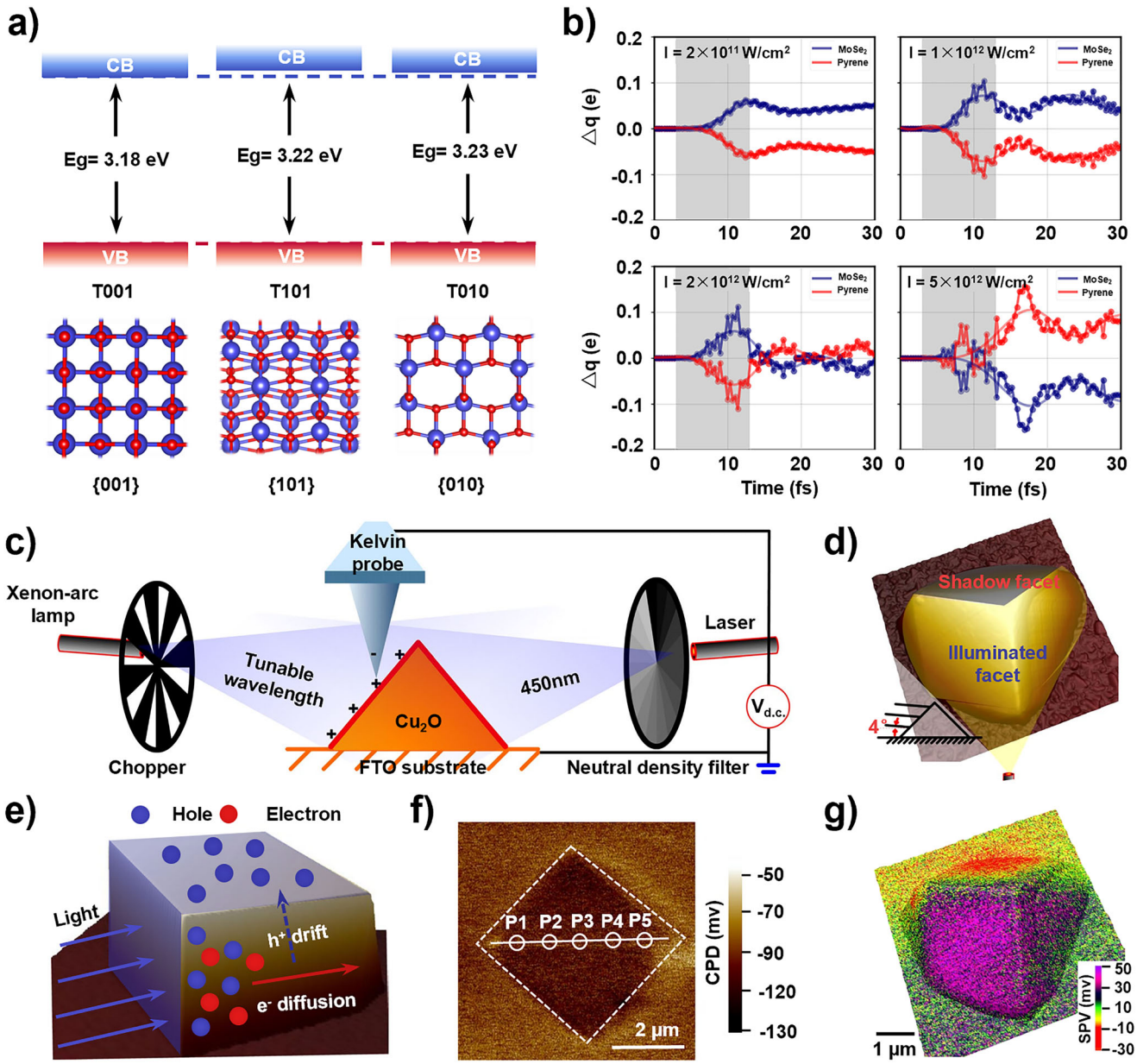

Figure 5. Anisotropic characteristics of the single-crystal semiconductors during the light energy trapping phase. a) The surface atomic composition of TiO_2, which defines the valence and conduction band edges of T001, T101, and T010. Copyright 2011, Wiley-VCH Verlag GmbH & Co. KGaA, Weinheim.[15] b) Variation of Bader partial charge relative to the ground-state value (Δq) with time under different laser intensities. The hybrid interface is partitioned into inorganic ($MoSe_2$) and organic (pyrene) components. Positive (negative) Δq values indicate electron accumulation (depletion). Gray shading indicates the duration of laser irradiation. Copyright 2022, American Chemical Society.[67] c) Experimental set-up for SPV imaging of the Cu_2O photocatalyst. Two light sources with a tunable light intensity and opposite irradiation direction were employed to perform the asymmetric photoexcitation. d) Illustration of asymmetric-irradiation-induced illuminated and shadow regions on a typical cubic Cu_2O particle grown along the (111) orientation. e) Illustration of the charge separation on the {001} facet parallel to the light irradiation direction. f) KPFM image of a typical Cu_2O particle grown alone the (001) orientation. g) SPVM image of the particle obtained by subtracting the surface potential in the dark from the surface potential under illumination. Copyright 2018, Macmillan Publishers Limited, part of Springer Nature.[24]

on overall photocatalysis remains challenging. Nonetheless, quantifying and modeling this influence is an inevitable step in the development of a comprehensive photocatalytic framework. Furthermore, it is worth noting that the directional optical response and anisotropic excitation dynamics of single-crystal semiconductors can be further amplified in low-dimensional heterointerfaces, where coherent light–matter interactions lead to nontrivial charge redistribution. A compelling demonstration of this concept is provided by Jacobs et al. through first-principles real-time time-dependent density functional theory (RT-TDDFT) simulations of a prototypical hybrid heterojunction composed of a $MoSe_2$ monolayer and physisorbed pyrene molecules (Figure 5b). Upon excitation with femtosecond laser pulses resonant

with molecular transitions, the system exhibits an intensity-dependent, time-resolved charge transfer across the interface. At low field strengths ($I = 2\times10^{11}$ W cm^{-2}), electron transfer proceeds unidirectionally from the photoexcited organic donor to the inorganic acceptor, consistent with the ground-state type-I band alignment. However, at higher excitation intensities ($I \geq 5\times10^{12}$ W cm^{-2}), this directionality reverses, leading to a net charge transfer from $MoSe_2$ to pyrene. This reversal is attributed to the saturation of available conduction band states in $MoSe_2$ and Pauli blocking effects, which hinder further electron injection from the donor and instead facilitate backflow of charge carriers. This finding highlights the critical role of excitation intensity and quantum-state occupancy in dictating interfacial charge dynamics under strong optical driving.[67] Evidently, unlike ground-state DFT or linear-response TDDFT, RT-TDDFT enables the explicit time evolution of electron density under time-dependent external perturbations such as pulsed light fields. This allows in silico tracking of transient processes including charge separation, relaxation, and directional carrier transport with sub-femtosecond temporal resolution. In anisotropic semiconductors, where direction-dependent excitation and carrier dynamics critically influence catalytic performance, RT-TDDFT provides predictive insights into facet-specific excitation probabilities, real-space charge delocalization, and field-driven carrier trajectories. These capabilities offer valuable guidance for the rational design of spatially optimized photoactive interfaces.

3.2. Extrinsically Induced Anisotropic Absorption

In addition to intrinsic facet-dependent absorption, artificially engineered asymmetric illumination offers a promising strategy for enhancing directional light absorption and charge separation in anisotropic photocatalysts. Under non-uniform illumination, such catalysts exhibit spatially diffusive charge separation, known as the Dember effect, arising from the difference in electron and hole mobilities (Figure 5c). In highly symmetric Cu_2O photocatalysts, for instance, asymmetric illumination enhances charge separation by driving holes toward the illuminated surface while directing electrons to the shadowed region (Figure 5d–g). This effect can be dynamically modulated by externally applied electric fields, enabling tunable anisotropic light absorption and introducing a novel charge separation mechanism.[24]

The concept of externally driven anisotropic illumination introduces a novel and thought-provoking strategy in photocatalysis. From a practical perspective, this illumination approach offers several key implications. First, spatially non-uniform excitation can enhance directional charge separation via the Dember effect, particularly in symmetric semiconductor structures, thereby suppressing charge recombination and improving overall quantum efficiency. Second, the deliberate introduction of light gradients mimics the naturally uneven distribution of sunlight, offering bioinspired design insights for photocatalytic systems, such as gradient-structured thin films or anisotropic reactor geometries. Third, when integrated with other external fields, anisotropic illumination enables the construction of multi-field coupling systems, allowing for real-time modulation of carrier dynamics and spatially programmable reaction zones. Fourth, this strategy facilitates a more realistic simulation of photocatalytic behavior under operational conditions, bridging the gap between idealized laboratory tests and solar-driven outdoor environments. In summary, the exploration of anisotropic illumination presents significant potential for advancing the field and warrants further in-depth investigation.

4. Anisotropy of Charge Separation and Transport

Most photocatalysts, particularly metal oxide semiconductors, suffer from inherently short carrier lifetimes (on the order of nanoseconds), limited diffusion lengths (typically a few nanometers), pronounced recombination, and defect trapping events.[74] These limitations fundamentally constrain the separation and transport of photogenerated charge carriers, which are critical for driving surface reaction kinetics. While considerable research has predominantly focused on the overall charge separation efficiency of the material, often overlooking the anisotropic nature of carrier migration, trapping, and transport across different crystal facets.

Recent advances in time-resolved spectroscopy, electric field-modulated scanning probe microscopy, and in situ characterization techniques have revealed that variations in electronic structure, built-in electric fields, and facet-dependent defect distributions establish localized driving forces that selectively govern charge carrier trajectories.[28–30] These findings indicate that photogenerated electrons and holes exhibit preferential migration pathways along certain crystallographic orientations, while in other directions they are more prone to undergo recombination or deep-level trapping. As illustrated in Figure 6a, Li and Fan's group demonstrated facet-specific ultrafast hot-electron transfer and anisotropic carrier trapping dynamics spanning timescales from sub-femtoseconds to microseconds.[25,72] In semiconductor photocatalysts, the directionality of charge migration across different surface facets is primarily governed by crystallographic structure, electronic band alignment, built-in electric fields, carrier mobility anisotropy, facet-dependent surface states, and defect distributions. A deeper understanding of these underlying mechanisms is essential for the rational design of high-performance photocatalysts, enabling precise control over charge separation and reaction kinetics at the atomic and mesoscale levels.

4.1. Inter-Facet Synergistic Effect

The synergistic effect of crystal facets serves as an intrinsic driving force for anisotropic charge carrier separation. Different facets exhibit distinct surface energies, electronic structures, and defect densities, which collectively dictate charge separation dynamics. The energetic disparity in band edge positions between these facets inherently drives the directional migration of photogenerated charges.[75] In this

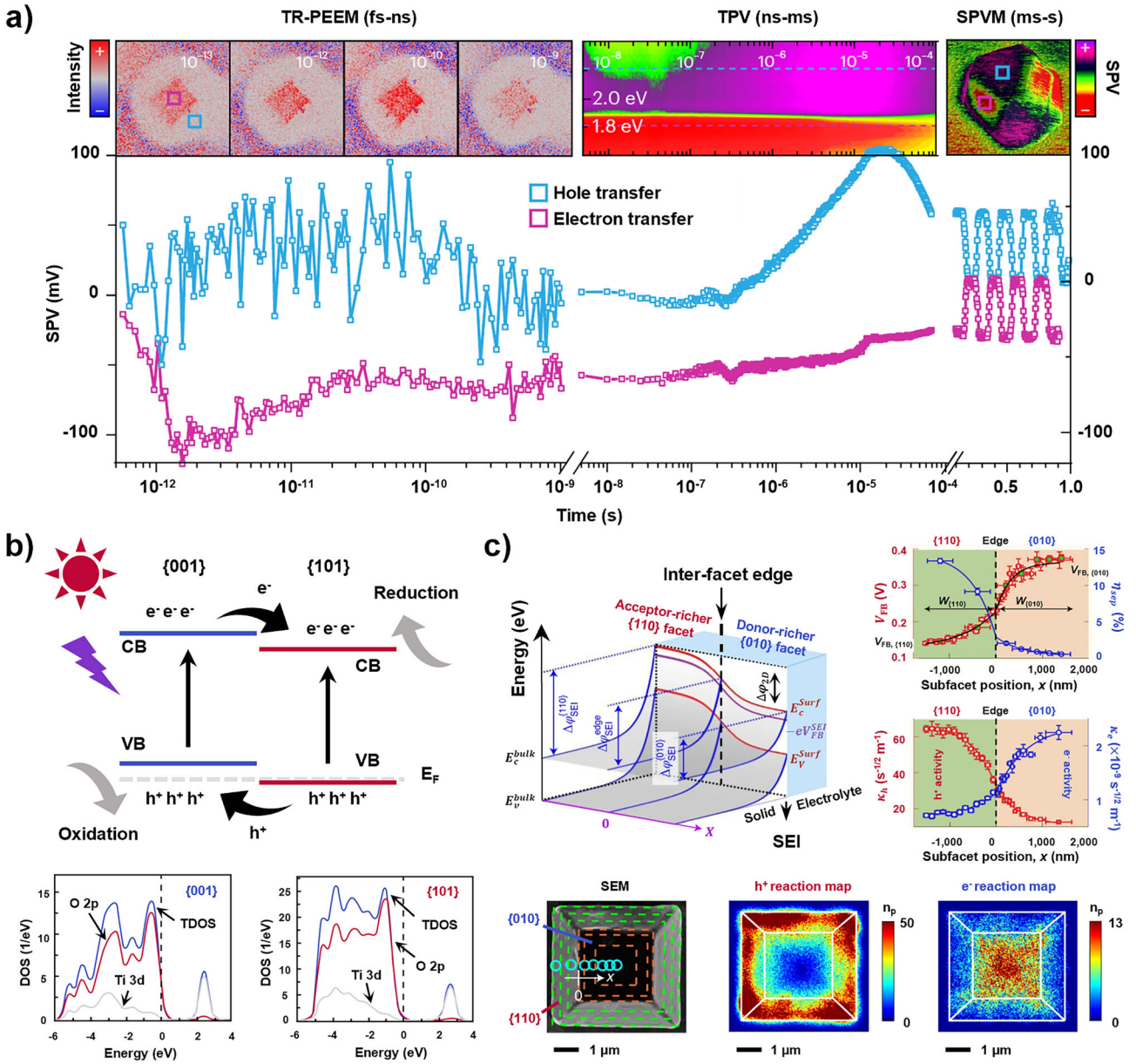

Figure 6. Dynamic tracking of separation and transport processes of photogenerated charges from fs to ms perspectives across the single-crystal interface (up); conceptual modeling of surface heterojunctions in charge separation (down). a) Tracking of electron and hole migration to surface reaction centers in individual single-crystal photocatalyst particles using time-resolved photoemission microscopy, transient surface photovoltage spectroscopy, and surface photovoltage microscopy. Copyright 2024, Spring Nature.[72] b) Schematic diagrams of surface heterojunctions of anatase TiO_2 {001} and {101}, and density of states (DOS) plots of the {101} and {001} surfaces. O 2p, Ti 3d, and TDOS represent the partial dos of O 2p, partial dos of Ti 3d, and total DOS, respectively. Copyright 2014, American Chemical Society.[17] c) Envisioned energy diagram demonstrating inter-facet junction effects in an anisotropically shaped $BiVO_4$ particle in contact with an electrolyte and key characterization of charge separation. SEI, solid-electrolyte interface. Copyright 2022, Spring Nature.[73]

context, inter-facet synergistic effect -induced anisotropic charge separation plays a pivotal role in enhancing quantum efficiency and facilitating spatially separated redox reactions.

The pioneering work by Majima et al. employed total internal reflection fluorescence microscopy (TIRF) in combination with single-molecule fluorescent probes to explore catalytic synergy among different crystal facets of TiO_2 at the single-molecule level. Fluorescence signals were predominantly concentrated on the {101} facets, providing direct visual evidence that photogenerated electrons preferentially migrate from {001} to {101}. This work challenged the conventional focus on high-surface-energy facets and, for the first time, emphasized the importance of inter-facet synergy in optimizing the spatial distribution of charge carriers.[14] To explore the pronounced spectral differences between crystal facets, our group further utilized micro-Raman mapping on anatase TiO_2 single crystals with a high fraction of exposed (001) facets, demonstrating that facet-specific anisotropy is closely associated with local lattice defects, such as oxygen vacancies and anharmonic distortions.[76] Building on this

foundation, Yu et al. further clarified inter-facet interactions and introduced the concept of surface heterojunctions (SHJs) (Figure 6b). Comparative studies on anatase TiO_2 with varying {001}/{101} facet ratios demonstrated that anisotropic charge carrier transport originates primarily from differences in band alignment, leading to SHJ formation and enhanced spatial charge separation along distinct migration pathways. However, when the {001} facet content exceeded 72%, electron migration to {101} became inefficient, resulting in excessive accumulation on {001}, which intensified electron-hole recombination. These findings highlighted the necessity of optimizing facet ratios rather than simply increasing the exposure of high-surface-energy facets to improve charge separation efficiency.[17]

Despite this progress, limitations in theoretical calculations and experimental characterization techniques had long restricted investigations of inter-facet synergy to the micrometer (μm) scale, preventing a detailed understanding of charge transport behavior at the nanoscale. Recently, Chen et al. utilized facet-resolved photoelectrochemical imaging and high-resolution potential mapping to investigate the inter-facet junction effects in anisotropic $BiVO_4$ single crystals with co-exposed {010} and {110} facets.[73] Their study revealed that the interface between these crystallographically distinct facets forms a lateral built-in junction, inducing facet-dependent band bending and driving anisotropic charge separation across the crystal surface. Super-resolution photocurrent mapping showed enhanced carrier collection localized at the junction edge, while scanning probe measurements demonstrated extended variations in flat-band potentials and local photovoltage on both sides of the junction (Figure 6c). Notably, these junction effects spanned micrometre-scale distances, well beyond conventional depletion widths. More importantly, high-resolution characterization unveiled a three-phase dependence of inter-facet charge carrier transport across different $BiVO_4$ crystal sizes. In small crystals (<3.5 μm), surface energy dominates, leading to severe electron-hole recombination. For intermediate-sized crystals (3.5–8.3 μm), inter-facet synergistic effects become more pronounced, enhancing directional charge migration efficiency. In large crystals (>8.3 μm), bulk-phase transport takes precedence, altering charge migration pathways. This work establishes inter-facet junctions as a powerful new design parameter for tuning the local photoelectrochemical landscape of single-crystal semiconductors beyond traditional facet exposure strategies.[73] Interestingly, the inter-facet junction effect is not confined to interactions between two facets. By leveraging specific crystal structures to introduce cascade charge transfer pathways, charge transport routes can be extended, optimizing carrier migration pathways and enhancing overall transport efficiency. As exemplified by eighteen-faceted BiOCl, where electrons preferentially migrate from {112} to {102} and subsequently to {001}, forming a cascade charge flow with superior separation efficiency compared to binary heterojunctions.[77]

Notably, inter-facet synergy engineering not only influences charge carrier transport across different crystal facets, but also plays a critical role in reducing the Schottky barrier, enhancing electronic coupling, and minimizing charge transfer resistance, thereby optimizing charge flow at both semiconductor–metal and semiconductor–reactant interfaces. For instance, in the $BiVO_4$ photoelectrochemical water oxidation system, coating the $BiVO_4$ photoelectrode with liquid metal while optimizing the {010}/{110} facet ratio to 53% significantly enhanced charge transport performance. At this optimal facet ratio, the {110} facet exhibited highly efficient unidirectional photogenerated electron migration to liquid metal, in contrast to the disordered electron transport pathways observed at other facet ratios.[78,79] Furthermore, the facet-junction-driven directional charge transport effect has garnered significant attention across multiple fields. In plasmonic catalysis, microfacet engineering has been employed to optimize the electronic states at plasmonic metal–molecule interfaces, thereby enhancing the direct interfacial transfer efficiency of hot carriers.[80] Even in perovskite thin films, precise control over the exposure ratio of {111} facets has been utilized to leverage their superior moisture resistance, stabilizing the moisture-sensitive {100} facets and significantly improving the environmental stability of the device.[81]

4.2. Built-in Electric Field

Engineering built-in electric fields to direct the transport of photogenerated charge carriers has emerged as a widely adopted strategy to improve carrier separation and transfer efficiency in photo(electro)catalytic systems. Traditionally, such internal fields originate at the interfaces of heterojunctions, such as semiconductor–semiconductor or semiconductor–metal contacts, where disparities in work function, Fermi level alignment, or doping concentration induce interfacial band bending.[53,82] In the context of single-crystal particles with anisotropic surface terminations, built-in electric fields originate from the redistribution of charge carriers near the surface, particularly due to interactions between surface states and bulk carriers. When surface traps capture majority carriers, such as electrons in n-type materials, a space charge region forms beneath the surface. This region is characterized by band bending and an electrostatic potential that typically points from the bulk toward the surface, acting as directional driving forces that promote spatial separation of carriers and suppress charge recombination. In the materials featuring asymmetric surface structures, both the magnitude and vectorial direction of the internal field vary with crystallographic orientation, enabling directional carrier migration across distinct crystal facets.[21,83] Unlike surface heterojunctions, where the field is confined to interfacial regions due to band offsets, the built-in electric field within anisotropic single crystals is governed by material polarization, space charge layers, and surface dipole layers that extend deep into the crystal bulk. Importantly, the strength and orientation of these internal fields can be finely modulated through the introduction of surface defects, cocatalysts, or engineered junctions on selected facets. This tunability enables the rational design of directional internal electric fields, offering a powerful means to enhance vectorial carrier transport and elevate the overall efficiency of photocatalytic energy conversion.

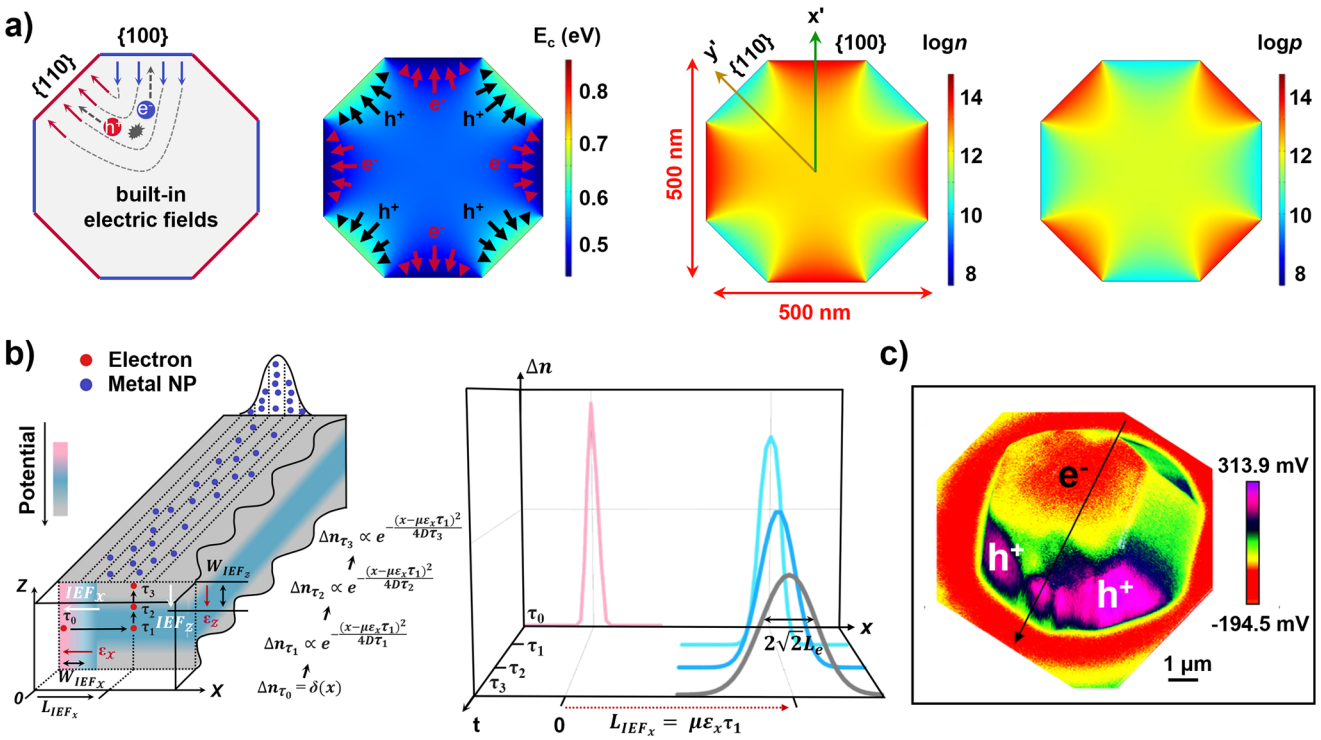

Figure 7. Conceptual model and related characterization of charge separation in built-in electric fields. a) Schematic illustration of photocarrier separation driven by built-in electric fields at the cross section and simulations of photocarrier distributions in $SrTiO_3$: Al single crystal particles. Copyright 2020, Spring Nature.[10] b) Schematic illustration of the cross-section of a platelet showing the migration pathway of photo-generated electrons driven by two intrinsic electric fields (horizontal and vertical). the directions of the intrinsic electric fields are indicated by red arrows, along with the spatial distribution profile of electrons at different time sequences. Copyright 2022, Spring Nature.[84] c) SPVM images of Sc–TiO_2 particles, illustrating anisotropic structure leads to surface-dependent charge distribution. Copyright 2025, American Chemical Society.[53]

The intrinsic variation in work function across different crystal facets of a single-crystal semiconductor induces an anisotropic internal electric field, which facilitates the directional migration of photogenerated electrons and holes toward distinct surfaces. This type of built-in field, which forms entirely within the crystal bulk, differs fundamentally from the interfacial electric fields observed in heterostructures such as semiconductor–metal junctions. Because it operates without involving interfacial charge transfer, it minimizes energy losses and provides a more efficient driving force for charge separation. Notably, even small differences in work function can generate a substantial effect on carrier dynamics. Domen and colleagues demonstrated through computational modeling that $SrTiO_3$: Al crystals exposing (100) and (110) facets exhibit pronounced anisotropic charge separation (Figure 7a), despite the work function difference between the facets being only around 0.2 eV.[10] Building upon this, our group has shown that by rationally tuning the exposed facets of $SrTiO_3$, the work function disparity can be further amplified. For instance, co-exposure of the (111) and (100) facets can result in an inter-facet electrostatic potential difference approaching 1 eV,[49] significantly enhancing the directional transport of charge carriers within a single photocatalyst particle.

In addition to facet engineering, the selective anchoring of redox cocatalysts offers a robust strategy for modulating charge carrier dynamics within single-crystal photocatalysts. The deposition of cocatalysts on specific crystal facets enables not only the directional migration of photogenerated electrons and holes toward distinct reactive sites but also the formation of interfacial dipoles that modulate local surface potentials. For instance, facet-specific loading of Pt@Au core–shell cocatalysts on the {101} facet of $Y_2Ti_2O_5S_2$ (YTOS) has been shown to induce internal electric fields as strong as 250 kV m^{-1}.[20] A dual-cocatalyst approach, where MnO_x and Pt are selectively positioned on the {011} and {010} facets of $BiVO_4$ respectively, further intensifies this effect, yielding an interfacial electric field reaching up to 2.5 kV cm^{-1}.[28] These findings highlight the synergistic potential of combining crystallographic anisotropy with surface functionalization to enhance built-in field-driven charge separation. Beyond cocatalyst engineering, built-in electric fields can also be reinforced through selective ion adsorption onto crystal facets with opposing surface charges. In N-doped TiO_2 nanoparticles, designed for photocatalytic seawater splitting, Na^+ ions preferentially adsorb onto the electron-rich {101} facet, reducing its work function and shifting the conduction band upward. Simultaneously, Cl^- ions accumulate on the hole-rich {001} facet, increasing the work function and lowering the valence band position.[85] This asymmetric ion distribution strengthens the internal electric field across the particle and offers a chemically accessible means of tuning carrier dynamics. Notably, such field modulation can be readily achieved by adjusting the electrolyte composition or pH,

providing a simple yet effective handle for optimizing charge separation.[34] Complementary to these intrinsic strategies, the application of an external electric field introduces a dynamic avenue for modulating carrier behavior in real time. Using single-molecule fluorescence microscopy with high spatiotemporal resolution, Tang and coworkers visualized, for the first time, the redistribution of photogenerated charge carriers under an external electric field.[34] Their observations reveal that the applied field not only perturbs band bending but also actively redirects carrier migration across anisotropic facets, offering deep insight into the field-responsive nature of single-particle photocatalysts.

The intrinsic crystal structure provides a fundamental basis for the presence of built-in electric fields within the bulk of single-crystal semiconductors. However, the behavior of photogenerated charge carriers under the influence of these internal fields is inherently vectorial in nature. Both the directionality of the electric field and the migration pathways of carriers cannot be fully explained by surface work function differences alone. Particularly within single-crystal systems, carrier transport characteristics can vary significantly depending on crystallographic orientation, making it necessary to develop intuitive and quantitative models to understand how built-in electric fields regulate anisotropic charge transfer dynamics. As shown in Figure 7b, Luo and coworkers addressed this challenge by constructing a mathematical model based on the Haynes–Shockley framework using BiOBr platelets as a model system. Their simulation incorporated dual electric fields along the X and Z directions within a single particle and revealed how different regions of the crystal respond dynamically to internal fields. By quantifying both the diffusion length and drift distance of electrons, they found that the spatial distribution of carriers migrating from the bulk to the surface under the influence of the internal field follows a Gaussian profile. Furthermore, they proposed that the size of the single-crystal particle should be commensurate with the carrier drift distance to optimize anisotropic charge separation driven by the built-in field.[84] Despite substantial progress, a complete and real-time understanding of anisotropic charge carrier dynamics within single-crystal photocatalysts remains a significant challenge. Developing realistic and predictive models of carrier transport requires the integration of multiple factors, including recombination kinetics, spatial heterogeneity in internal electric field strength, and dynamic behavior across varying timescales. These complexities are essential to accurately describe the full trajectory of photogenerated carriers within individual catalyst particles.

Notably, a recent study by Liu's team on single-particle, single-crystal semiconductor systems employed SPVM and KPFM to provide direct experimental evidence of anisotropic charge separation across different crystal facets in Sc-doped TiO_2.[53] Compared to conventional characterization techniques that yield spatially averaged or time-invariant data, the combination of SPVM and KPFM enables direct, real-space measurement, and quantification of built-in electric field strengths. This high-resolution approach allows for precise mapping of charge localization and migration pathways across distinct crystal facets, offering deeper insight into facet-dependent charge dynamics (Figure 7c). By correlating local surface potentials with specific structural domains, offers valuable insights into how facet orientation and internal electric fields influence the directional transport of charge carriers.[21,83] It further provides essential technical guidance for optimizing built-in electric field-induced anisotropic charge separation pathways, through material design strategies including crystal facet engineering, cocatalyst integration, and defect modulation.

Furthermore, ferroelectric materials, owing to their intrinsic ferroelectric (or piezoelectric) polarization effects, naturally possess built-in electric fields. Theoretically, the photovoltage generated in ferroelectrics can exceed that of solar cells, making them emerging candidates for photocatalysis. For example, Liu et al. reported that single-domain $PbTiO_3$ exhibits facet-dependent built-in electric fields on the corresponding {100} facets, which can be explicitly confirmed by cocatalyst photodeposition experiments. Similarly, $PbTiO_3$ has been found to exhibit a built-in electric field extending throughout the entire crystal.[88] However, the efficiency of ferroelectric photocatalysts remains relatively low, possibly due to their limited surface states and insufficient catalytic reaction sites. Moreover, their short electron diffusion lengths and typically large crystal sizes result in low charge carrier mobility. Therefore, the exploitation of anisotropic charge separation arising from intrinsic asymmetry in ferroelectric materials remains largely unexplored and holds significant potential for future development.

4.3. Carrier Mobility Along Crystal Orientations

In single-crystal photocatalysts, the anisotropic mobility of charge carriers along different crystallographic directions is an inherent property governed by the intrinsic crystal structure. This directional driving force is fundamentally distinct from interfacial junction effects and built-in electric fields, which arise from variations in surface potential. The diffusion distance of photogenerated charge carriers refers to the average distance a photoexcited carrier can travel before recombination. A longer diffusion distance, typically enabled by high mobility, is essential for achieving efficient photocatalytic reactions. This parameter is generally determined by the mobility and lifetime of the charge carriers.

The carrier mobility (μ) can be described by the classical Drude model, as shown in Equation (2):

$$\mu = \frac{e\tau}{m^*} \tag{2}$$

where e denotes the elementary charge, τ is the mean scattering time, and m^* represents the effective mass of the charge carrier.

Notably, the effective mass (m^*) is one of the key parameters governing the mobility of photogenerated carriers: the smaller the effective mass, the higher the mobility. It has been proposed that, to achieve efficient carrier transport, the effective mass should ideally be less than 0.5 m_e, where m_e is the free electron mass.[89] However, most complex metal oxides exhibiting d-band conduction possess

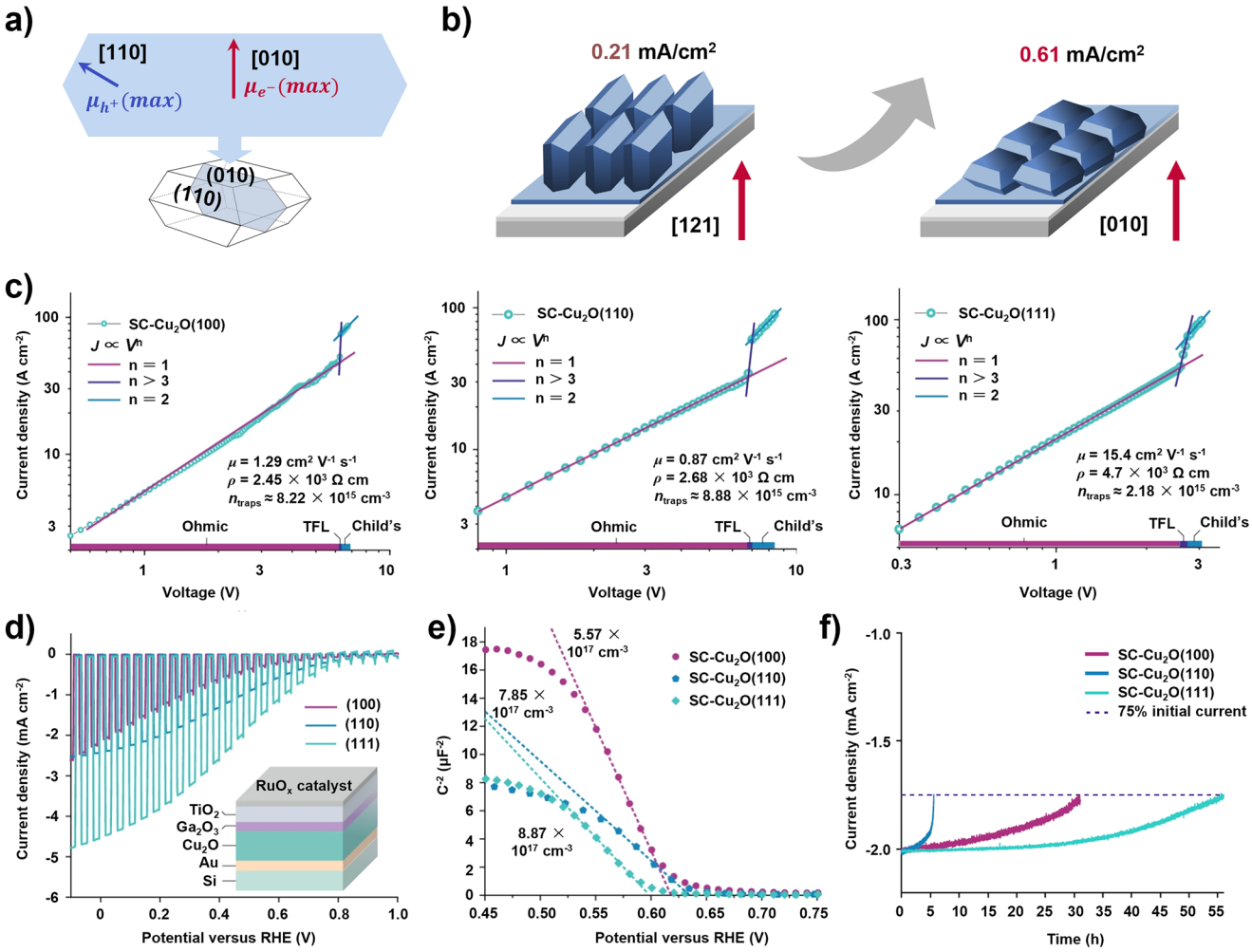

Figure 8. Mechanism of anisotropy of electron-hole migration along the orientation in single-crystal thin-film photoelectrodes. a) Differences in electron-hole transport rates along the crystal axis [*hkl*] and the corresponding face (*hkl*) in $BiVO_4$. Copyright 2015, Royal Society of Chemistry.[86] b) Schematic representation of the change in $BiVO_4$ photoanode growth array (from perpendicular to parallel) and the corresponding change in photocurrent density. Copyright 2019 American Chemical Society.[87] c) Current density–voltage curves of hole-only devices with SC-Cu_2O(100), SC-Cu_2O(110), and SC-Cu_2O(111). d) PEC responses of SC–Cu_2O photocathodes for solar hydrogen evolution under a simulated one-sun condition. The inset shows the layered structure of the Cu_2O photocathodes. e) Mott–Schottky plots of SC–Cu_2O thin films tested in pH 9 carbonate buffer solution. The carrier densities were calculated based on the slopes of the linear fitting represented by the dotted lines. f) Stability test on SC–Cu_2O photocathodes with a 20 nm TiO_2 layer biased at various potentials to each deliver an initial current density of 2 mA cm^{-2} (SC–Cu_2O(100) at 0.03 V versus the RHE, SC–Cu_2O(110) at 0.21 V versus the RHE, SC–Cu_2O(111) at 0.48 V versus the RHE) using chronoamperometry techniques. All measurements with SC–Cu_2O were ceased when the photoelectrodes lost 25% of their initial photocurrent. Copyright 2024, Spring Nature.[26]

significantly larger effective masses, typically ranging from 1 to 10 m_e, thereby imposing substantial limitations on carrier mobility.[90] Theoretical studies by Li et al. proposed that electron mobility is significantly higher than hole mobility in the same crystallographic direction (Figure 8a). However, when the {010} and {110} facets of $BiVO_4$ are highly exposed, the electron mobility along the [010] direction reaches a maximum of 0.226 eV, while the hole mobility along the [110] direction reaches 0.433 eV.[86] This pronounced anisotropy in carrier mobility, induced by facet exposure, suggests a parallel relationship between carrier migration along crystallographic axes and preferential accumulation on corresponding crystal facets. The variation in electron mobility with respect to crystallographic direction correlates with the accumulation of carriers on the corresponding facets. The charge distribution along the [*hkl*] axis (or vacancy) is likely related to charge separation between the corresponding (*hkl*) facets. When surface factors such as band bending and surface energy differences come into play, the electron (or hole) mobility along the [*hkl*] axis reaches its maximum, leading to the preferential accumulation of photogenerated electrons (or holes) on the corresponding (*hkl*) facets.

The anisotropic carrier migration effect induced by crystal orientation becomes particularly pronounced under an external force field, such as in photo(electro)catalysis, where the applied electric field significantly enhances carrier migration efficiency along specific crystal orientations. For instance, the photocurrent density of a $BiVO_4$ photoanode with a preferential [010] orientation is 2.9 times greater than that of a [121]-oriented electrode (Figure 8b). By optimizing

crystal orientation, the migration pathways of electrons and holes can be precisely controlled, ensuring efficient transport to catalytic sites before recombination.[87] This anisotropic carrier mobility along specific crystal orientations can be further enhanced through surface engineering or external modifications. Wang et al. employed a simple electrochemical treatment, the partial reduction of Bi^{3+} and V^{5+} ions in $BiVO_4$ generates oxygen vacancies, enhancing both bulk and surface charge separation. Additionally, the cocatalyst modification further accelerates surface reaction kinetics, resulting in a threefold increase in carrier density.[54] In most single-crystal semiconductor photocatalysts, photogenerated electrons or holes tend to exhibit superior mobility along specific crystallographic orientations. For instance, in WO_3, the {110} facet demonstrates significantly higher carrier mobility than the {001} facet.[91] More recently, Pan et al. addressed the intrinsically limited carrier diffusion distance in copper oxide by fabricating high-purity polycrystalline Cu_2O films with a preferential (111) crystallographic orientation, leveraging the anisotropic carrier mobility in different crystal directions. The anisotropic carrier transport in single-crystal Cu_2O films was systematically investigated for the first time, with precise quantification of electron and hole transport distances along different crystallographic directions. When charge transport is directed along the [111] orientation, the carrier diffusion distance increases by more than an order of magnitude compared to random diffusion (Figure 8c). A photocurrent density of 7 mA cm^{-2} was achieved at a critical potential of 0.5 V versus the reversible hydrogen electrode (RHE). As illustrated in Figure 8d–f, this improvement represents *a* >70% enhancement over the previous state-of-the-art electrodeposited Cu_2O photoelectrode, which also achieves a charge separation efficiency of 80%.[26]

Notably, the anisotropic nature of carrier-specific transport across different crystalline phases becomes more pronounced in nanostructures with high aspect ratios. The inherent anisotropy of high-aspect-ratio morphologies is particularly advantageous for this process, as the rod-like structure sustains charge separation for a sufficient duration to facilitate surface reactions. Selective growth of rod-shaped CdS enabled the spatial separation of two catalytically active sites: platinum nanoparticles were positioned at the tips, while ruthenium-based molecular catalysts were anchored on the side surfaces via dithiocarbamate (DTC) ligands.[92] Driven by the potential difference between the two sites, photogenerated electrons migrated toward the tip along the rod axis, while holes were transported to the side surfaces. This directional charge separation not only facilitated carrier migration along specific crystallographic orientations but also effectively suppressed electron-hole recombination.

Collectively, these findings underscore that precise control over crystal structure provides a powerful means to regulate charge transport pathways and suppress recombination. Anisotropic charge transport mechanisms should be designed based on favorable crystallographic orientations, further enhanced by built-in electric fields, and ultimately complemented by facet synergy effects to optimize interfacial charge transfer. This multi-faceted approach enables the realization of efficient and stable anisotropic charge separation and migration pathways, thereby significantly boosting PEC activity.

5. Anisotropy in Surface Reaction

In photo(electro)catalysis, the single-crystal semiconductor surface acts as a critical interface where photogenerated charge carriers drive redox reactions. The surface structure, composition, and crystallographic orientation dictate key catalytic properties, including reactant adsorption, intermediate stability, charge transfer kinetics, and product desorption. These factors underpin facet-dependent reaction selectivity, as different crystal facets favor distinct oxidation and reduction pathways due to variations in atomic coordination, electronic structure, and local reaction environments. Certain facets preferentially stabilize intermediates, lower activation barriers, or accumulate charge carriers, thereby shaping reaction kinetics and product distribution. To elucidate these facet-specific processes, fluorescent molecules and photodeposited metals or oxides serve as effective probes, selectively interacting with photogenerated electrons or holes. This enables precise mapping of redox-active sites, offering mechanistic insights into surface reaction dynamics.

5.1. Static Anisotropic Surface Reactivity

The surface interface of crystal facets, as the primary contact layer with reactants, directly influences the response of the reaction system. Therefore, optimizing the surface state can further enhance reaction efficiency, selectivity, and overall catalytic performance. Taking $SrTiO_3$ as an example, the (100) facet generally exhibits lower surface energy, facilitating hydrogen proton adsorption and electron accumulation, whereas the (110) facet demonstrates stronger oxidative capability, extending hole lifetimes. This anisotropic effect becomes even more pronounced upon cocatalyst loading. Domen et al. achieved an unprecedented 96% apparent quantum efficiency (AQY) for photocatalytic pure water splitting under ultraviolet light by leveraging anisotropic phase engineering of $SrTiO_3$ single crystals loaded with Rh/Cr_2O_3 and CoOOH.[10] This efficiency is close to the theoretical limit for maximizing photogenerated charge utilization. Similarly, as illustrated in Figure 9a,b, we found that on $SrTiO_3$ crystals exposing both {100} and {111} facets, the cocatalyst exhibits a pronounced facet-dependent selective deposition behavior. Using a photodeposition method, Rh/Cr_2O_3 nanoparticles were predominantly formed on the {100} facets in a core–shell configuration, serving as active sites for hydrogen evolution, whereas CoOOH preferentially loaded onto the {111} facets, functioning as oxidation sites for oxygen evolution.[49] Such facet-selective cocatalyst distribution enables spatial separation of reduction and oxidation reactions, promotes directional interfacial charge transfer, and simultaneously stabilizes high-energy facets by mitigating surface reconstruction or corrosion. Strategically anchoring oxidative cocatalysts on hole-rich, oxidation-prone

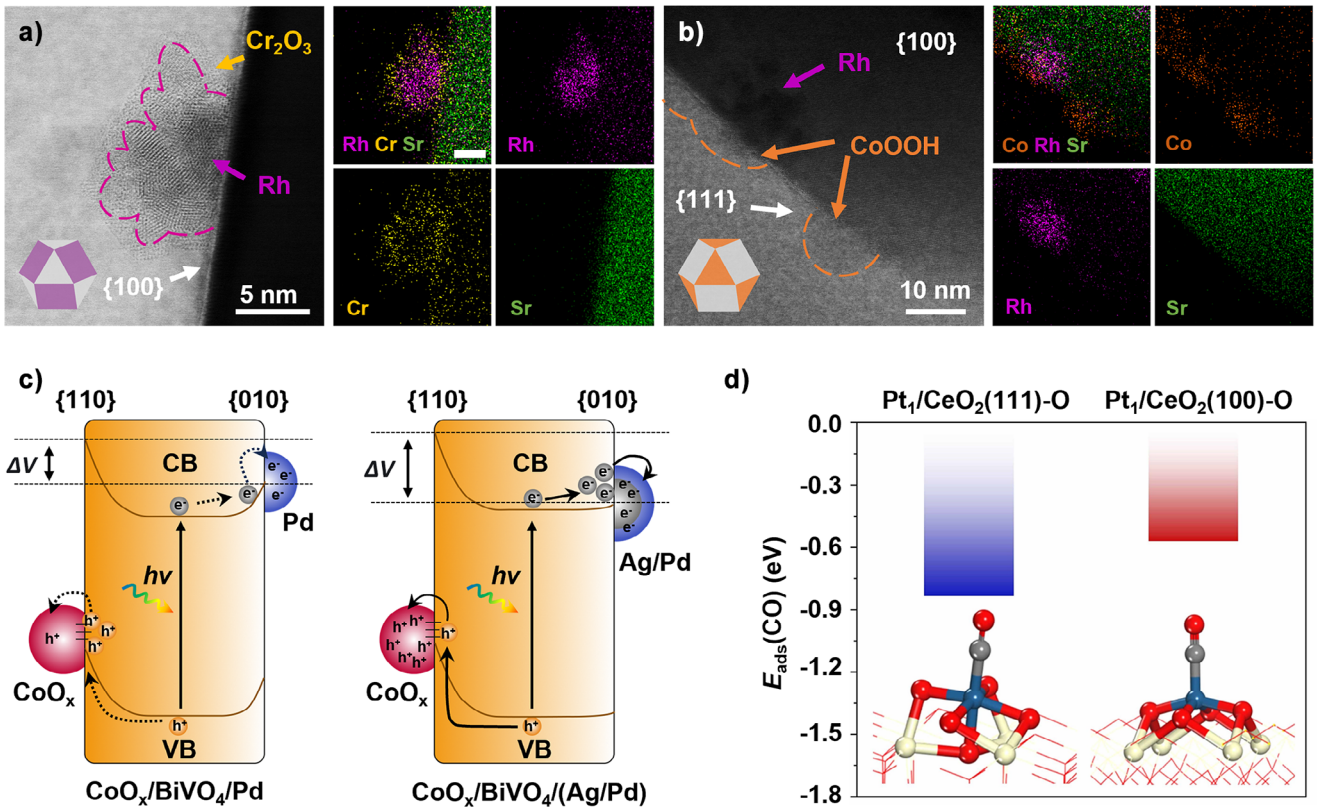

Figure 9. Anisotropic synergistic interaction between cocatalyst and facet-engineered catalyst. a), b) Bright-field STEM images and corresponding EDS maps, suggesting a clear core/shell structure Rh/Cr_2O_3 nanoparticle loaded on the {100} facet and CoOOH loaded on the {111} facet, functioning as oxidation and reduction sites, respectively. Schematic model with bright-colored facets indicating specific cocatalyst-loaded surfaces. Copyright 2024, American Chemical Society.[49] c) Schematic illustration of the charge-separation process enhanced by surface energetics tuning. Copyright 2022, Nature Publishing Group.[93] d) CO adsorption energies and configurations on Pt-decorated CeO_2 (111) and (100) facets. Copyright 2024, Wiley-VCH GmbH.[94]

facets can effectively suppress lattice degradation induced by photogenerated holes, while placing reductive cocatalysts on electron-accumulating surfaces helps prevent photocorrosion. For example, Fe enhances hole extraction through Fe—O—Bi bonding, while Ni suppresses V^{5+} leaching via Ni–O–V interactions.[95] The integration of Fe and Ni cocatalysts markedly improves both the photoelectrochemical activity and long-term stability of $BiVO_4$ photoanodes.

Beyond enhancing reaction efficiency and catalyst stability, cocatalyst also affects reaction selectivity, intermediate stability, and the adaptability of the catalyst surface to its environment. As illustrated in Figure 9c, tuning the interfacial energy using an Ag/Pd core–shell structure can significantly optimize the asymmetric energy driving force between reduction and oxidation sites.[93] Additionally, cocatalysts can be selectively loaded onto specific crystal facets according to reaction conditions, further optimizing facet-dependent surface reactions. The coordination environment and structural variation of cocatalysts on different facets lead to distinct catalytic effects. In CeO_2 tetrahedra nanocrystals, Pt atoms anchored on the {100}, {110}, and {111} facets exhibit distinct Pt—O coordination structures. For CO oxidation, Pt/CeO_2{100} provides the most active oxygen sites (Figure 9d), whereas Pt/CeO_2{111} strongly adsorbs O_2, exhibiting opposite characteristics.[94] Alternatively, controlling the local coordination structure of cocatalysts on the same substrate offers another pathway to modulate catalytic performance. For instance, an ice-templated strategy was employed to selectively deposit Ru cocatalysts with different coordination forms, including single atoms, atomic clusters, and nanoparticles, onto a narrow-bandgap $La_5Ti_2Cu_{0.9}Ag_{0.1}O_7S_5$ (LTCA) photocatalyst. Among these, Ru atomic clusters with a moderate Ru–Ru coordination number (approximately 3.4) exhibited a twofold to fivefold higher photocatalytic hydrogen evolution activity compared to isolated Ru single atoms and larger Ru nanoparticles.[96] Similarly facet-dependent anisotropy has been widely observed in model photocatalysts such as $BiVO_4$,[97] TiO_2,[98] and BiOBr.[99]

Defect engineering provides an additional dimension for modulating facet-dependent catalytic properties. One of the most widely studied defect effects in metal oxides is the formation and distribution of oxygen vacancies, which significantly influence charge carrier dynamics and surface reaction selectivity. For instance, in $BiVO_4$, the oxygen vacancy distribution exhibits strong facet dependence. Studies have shown that the {110} facet of $BiVO_4$ typically has a lower oxygen vacancy concentration than the {010} facet, leading to higher photogenerated hole energy levels on the {110} surface. Since the {110} facet also accumulates photogenerated holes, it becomes particularly favorable for

O_2 evolution.[100] To further refine this selectivity, Zheng et al. employed low-temperature plasma treatment and heterojunction construction to strategically introduce oxygen vacancies, thereby tuning their spatial distribution and selectively enhancing facet-dependent reactions.[29] Similarly, defect engineering has been widely applied in anatase TiO_2, where oxygen vacancies govern the charge distribution and adsorption strength of surface species. These vacancies also induce the formation of large electronic polarons, which play a crucial role in biomass-derived platform molecule transformation.[22,101] Therefore, the rational selection of catalysts with anisotropically exposed facets, combined with reactivity modulation through cocatalyst loading, defect engineering, and heterojunction construction, is crucial for directing reaction pathways and enhancing catalytic selectivity. Nonetheless, the development of model systems with well-defined surface properties tailored to specific reaction requirements remains a central challenge in the design of high-performance photo(electro)catalysts.

5.2. Dynamic Anisotropic Surface Processes

Traditionally, research on facet-dependent surface reactions has primarily focused on the static anisotropy of charge carrier distribution and catalytic activity on specific crystal facets. However, this static perspective overlooks critical dynamic processes, such as variations in surface carrier concentration and lattice distortions, which play a crucial role in governing reaction rates. These dynamic transformations significantly influence overall photocatalytic efficiency and must be considered for a comprehensive understanding and optimization of reaction kinetics.

Nevertheless, real-time experimental observation remains a formidable challenge, as advanced in situ characterization techniques are still in development. Fortunately, recent advancements in theoretical modeling have begun to address this gap. For instance, Wang et al. quantitatively analyzed the electron-hole separation efficiency on TiO_2 facets (Figure 10a). Their study revealed that the primary limiting factor in the oxygen evolution reaction (OER) is not the traditionally assumed O—O bond formation barrier but rather the low surface hole concentration (C_{h+}), which directly impacts the reaction rate.[102] In surface redox reactions, resolving the imbalance between electron and hole reaction rates is essential for improving overall catalytic performance. Regarding the long-standing debate on the migration pathways of photogenerated holes to the catalyst surface, Meng's group proposed two distinct mechanisms: field-driven water dissociation and hole-driven water dissociation. As illustrated in Figure 10b,c, their study established a polarization-assisted two-stage model for water dissociation, quantifying the time dependence of photocatalytic reactions. In the field-induced pathway, photoexcited electron transfer from bridging oxygen ($O_{br)}$) to the oxygen atom in adsorbed water (O_w) initiates a proton transfer to O_{br}, yielding terminal and bridging hydroxyl species that are stabilized by anisotropic surface coordination. In contrast, the hole-induced pathway involves in-plane orbital anisotropy, which facilitates hole-mediated water dissociation via polaron formation at Ti_{5c} and adjacent O_{3c} sites, triggering secondary deprotonation steps.[103]

Importantly, real-time time-dependent density functional theory (rt-TDDFT) simulations capture the coupled evolution of charge density and lattice relaxation, enabling atomistic-resolution insights into light-induced reaction pathways. However, experimental validation of such directional light–matter interactions remain challenging, primarily due to current limitations in spatiotemporal resolution and the inherent difficulty in disentangling intrinsic crystallographic anisotropy from externally imposed fields or illumination gradients. In the future, integrating emerging techniques such as the aforementioned time-resolved surface photovoltage (SPV) mapping with rt-TDDFT predictions may provide a promising synergistic framework for probing the dynamics of anisotropic charge carrier migration toward surface reactions. Building on this framework, recent DFT investigations further underscore the dynamic, facet-dependent behavior of reactive intermediates during activation. Specifically, on anatase TiO_2, compared to the {001} surface, the {101} facet facilitates an exothermic proton transfer ($\Delta E = -0.22$ eV) between adsorbed •OH species and interfacial H_2O, promoting rapid desorption of •OH into the liquid phase (Figure 10d). Concurrently, Pd^{2+} nanoclusters anchored on the {101} surface selectively stabilize mobile $•CH_3$ radicals and significantly lower the energy barrier for C–C coupling to C_2H_6 (0.48 eV), whereas isolated Pd atoms fail to support dual-site adsorption (Figure 10e). Furthermore, in the context of photocatalytic reaction selectivity, the electron trapping states on different TiO_2 facets play a crucial role. It has been found that electrons dynamically accumulate on distinct crystal facets, leading to differential trapping energies (Figure 11a–d). On the (101) facet, the shallow electron trap states facilitate CO formation via formic acid (FA) dehydration, whereas on the (001) facet, the deeper electron traps stabilize FA, favoring oxidation reactions.[105]

These findings underscore the growing emphasis on unraveling dynamic processes that govern surface reactions in photo(electro)catalysis, marking a paradigm shift beyond conventional static perspectives. Deepening the understanding of these reaction mechanisms is crucial for material design, enabling researchers to strategically optimize crystal size, facet exposure, surface defect engineering, and cocatalyst modifications to enhance catalytic performance.

6. Future Perspectives

In summary, anisotropic characteristics play a crucial role in driving reaction processes, from light absorption to surface catalytic transformations. Designing single-crystal semiconductor photocatalysts across multiple scales presents a promising strategy for maximizing photocatalytic efficiency. By optimizing light harvesting, leveraging crystallographic orientation effects, promoting efficient charge separation, ensuring sufficient carrier accumulation at active sites, and integrating facet-specific cocatalysts, it becomes possible to fully exploit anisotropy as a key design principle in catalysis. With the advent of artificial intelligence (AI),

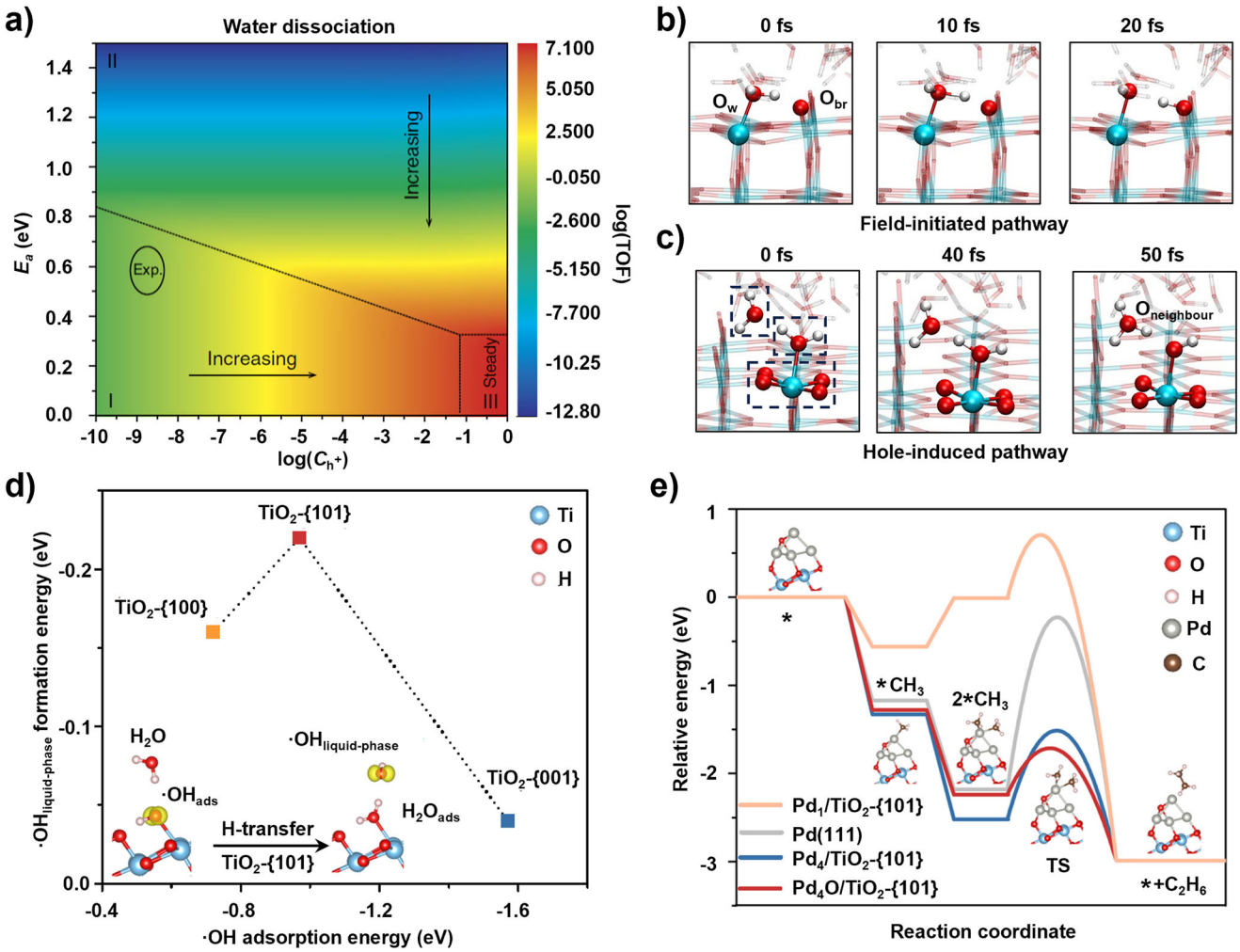

Figure 10. Theoretical elucidation of facet-dependent surface reaction mechanisms. a) TOF evaluation as a function of hole concentration based on hydrolysis-driven microkinetic analysis. Copyright 2018, Macmillan Publishers Limited, part of Springer Nature.[102] b), c) Atomic configurations at specific time points along field-driven and hole-driven pathways in photoinduced water dissociation processes. Copyright 2024, Springer Nature.[103] d) The liquid-phase •OH formation energy versus the •OH adsorption energy on anatase TiO_2 with different exposed facets. The inset displays the optimized structures for $\cdot OH_{liquid\text{-}phase}$ generation by H-transfer on TiO_2-{101} surface. e) The relative energy for the coupling of $\cdot CH_3$ to C_2H_6 on the model surfaces of Pd_1, Pd_4, andPd_4O loaded on anatase TiO_2-{101} as well as on the Pd(111) surface. The inset displays the optimized structures for $\cdot CH_3$ enrichment and self-coupling on Pd_4O site loaded on TiO_2-{101}. Copyright 2024, Springer Nature.[104]

photo(electro)catalysis research has entered a new era of "dynamic design". The integration of AI-assisted materials informatics with theory-driven microkinetic modeling now enables the rational development of full-spectrum catalysts spanning the ultraviolet to visible light range. However, advancing key applications, including cost-efficient solar water splitting for hydrogen generation, selective biomass conversion, and photo(electro)chemical synthesis, demands both technological innovation and the careful optimization of reaction pathways. As exemplified by the EU's Graphene Flagship project, true technological advancements can only be realized through the synergy of atomic-scale material innovations and system-level research under realistic operational conditions. The same paradigm must be applied to photo(electro)catalysis, where bridging fundamental material design with practical implementation will be essential for achieving transformative progress within the next decade. Therefore, the challenges and future directions will be profiled in the following sections.

6.1. Precise Control in Crystal Facet Engineering

The rational design and fabrication of semiconductor materials are fundamental to controlling their anisotropic properties, with single-crystal configurations and surface atomic arrangements forming the foundation for directional charge transport and reaction selectivity. Solid-state synthesis methods, particularly those enabling precise control over crystallinity, particle morphology, and defect distribution, have demonstrated unique advantages in preparing high-quality photo(electro)catalysts. High crystallinity not only enhances carrier mobility and suppresses recombination but also ensures structural stability under reaction conditions. Despite

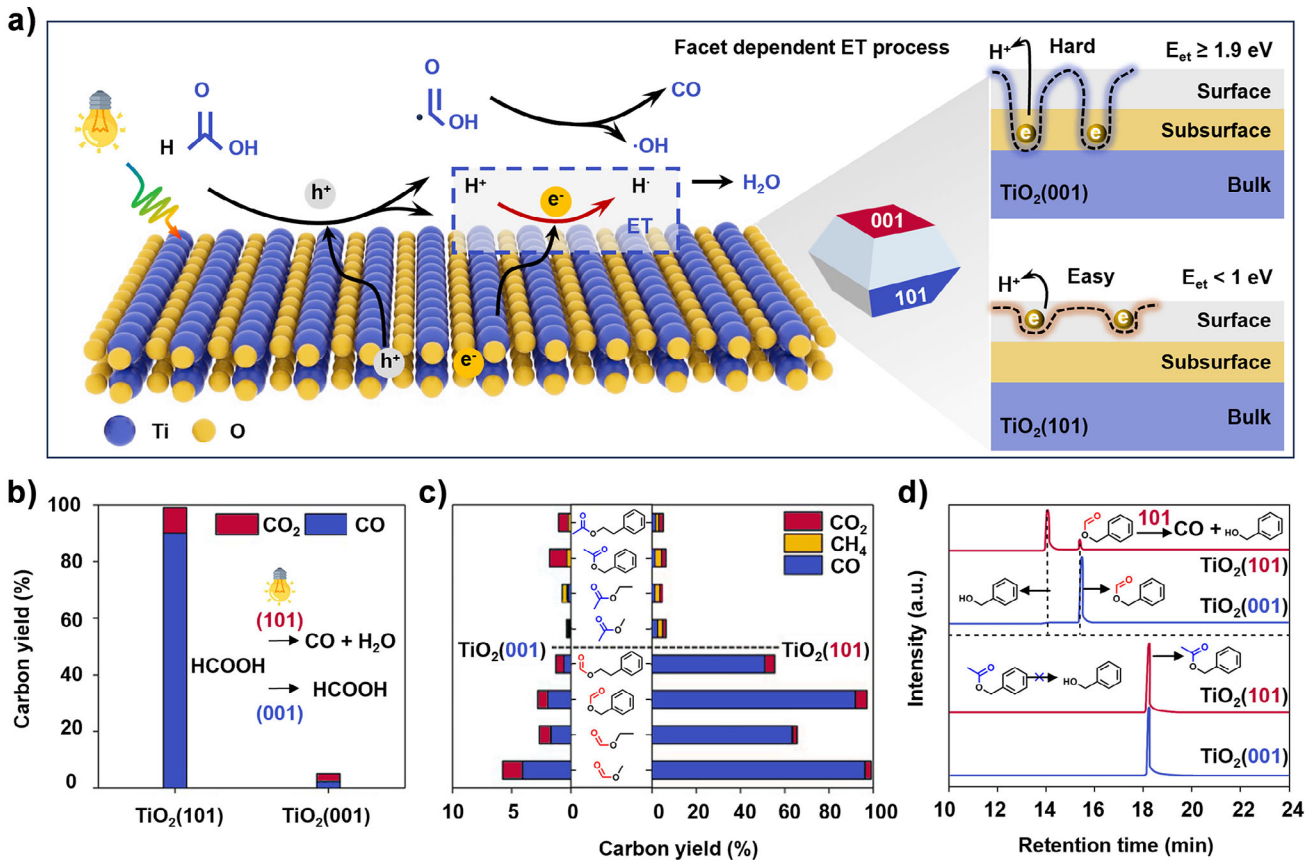

Figure 11. Anisotropy of surface reactions in facet-dependent photocatalysts. a) Scheme of photocatalytic FA decomposition over TiO_2. b) Photocatalytic dehydration of FA over TiO_2. c) Photocatalytic ester decomposition activity over TiO_2. d) Gas chromatography (GC-MS) results of the reaction liquid of benzyl formate and benzyl acetate. Copyright 2022, American Chemical Society.[105]

significant progress, achieving the large-scale, controllable synthesis of highly crystalline single-crystal semiconductors with exposed high-index facets or engineered anisotropy remains a formidable challenge. Advancing solid-state synthesis strategies, including templated growth, flux-assisted crystallization, and molten-salt routes, will be critical for future development.

6.2. Theoretical Modeling at the Single-Particle Scale

Alongside materials synthesis, theoretical modeling plays an increasingly pivotal role in deciphering anisotropic behaviors. Conventional computational methods often treat small clusters or periodic slabs, failing to capture the realistic complexity of large, anisotropic particles composed of tens of thousands of atoms. Future efforts should focus on the development of multiscale simulation frameworks capable of quantifying surface properties, defect distributions, and local charge dynamics, especially at the single-particle level. Such models should incorporate realistic facet junctions, doping distributions, and strain effects, enabling a comprehensive and quantitative description of anisotropic photo(electro)catalytic systems. Machine learning and data-driven approaches will further accelerate predictive modeling and guide experimental synthesis.

6.3. Facet-Specific Cocatalyst Loading and Atomic-Scale Doping Strategies

The spatially selective loading of cocatalysts onto specific crystal facets has emerged as a powerful strategy to optimize surface reactions, directly leveraging the intrinsic anisotropy of semiconductors. Building upon this foundation, further refinements at the atomic scale, such as anisotropic doping and interfacial engineering, are poised to unlock new dimensions of control. The ability to site-selectively introduce dopants or defect structures on specific facets or facet junctions can tailor local electronic structures, enhance charge separation, and modulate surface reaction pathways. Achieving precise anisotropic doping requires advances in both synthetic chemistry and characterization techniques capable of resolving dopant distribution at atomic resolution.

6.4. Advancements in Ultrafast and Spatially Resolved Characterization

The dynamic nature of photo(electro)catalytic processes demands characterization tools capable of capturing charge carrier generation, transport, and recombination across ultrafast timescales and at nanoscopic spatial resolutions. Current techniques primarily rely on ensemble

measurements, which obscure critical single-particle and single-event information. Future advancements must focus on developing characterization methods that achieve attosecond-level temporal precision and atomic-scale spatial mapping. Integration of techniques such as time-resolved photoelectron spectroscopy, single-particle fluorescence spectroscopy (SPFS), ultrafast transient absorption microscopy, and scanning probe microscopy will be essential. For instance, Li et al. elucidated key charge dynamic processes in Cu_2O photocatalysts across multiple timescales, ranging from quasi-ballistic electron transfer within 0.2 ps to defect-mediated hole trapping over nanoseconds.[25] Similarly, Zheng et al. utilized SPFS in combination with SEM/TEM to resolve local carrier dynamics within individual nanostructures.[29,106] These efforts provide a roadmap for future structure-dynamics-reaction correlation studies.

6.5. Integration of Artificial Intelligence (AI) in Material Discovery

The integration of AI-driven materials discovery with first-principles modeling opens new opportunities for rational anisotropic catalyst design. Data-driven models can predict favorable facet exposure conditions, guide doping strategies, and optimize cocatalyst architectures before experimental synthesis. Such integration will not only accelerate materials development but also allow for the rational exploration of vast compositional and structural spaces previously inaccessible through conventional trial-and-error methods.

Acknowledgements

This work was financially supported by the National Key Research and Development Program of China (No: 2024YFF0506203, 2023YFA1507102), the National Natural Science Foundation of China (22239001 and 22379043), the Shanghai Pilot Program for Basic Research (22TQ1400100-12), and the Science and Technology Commission of Shanghai Municipality (23520710700 and 25ZR1402129).

Conflict of Interests

The authors declare no conflict of interest.

Data Availability Statement

The data that support the findings of this study are available in the Supporting Information of this article.

Keywords: Anisotropy · Charge carrier dynamics · Facet engineering · Photo(electro)catalysis · Single-crystal

[1] T. S. Teitsworth, D. J. Hill, S. R. Litvin, E. T. Ritchie, J. S. Park, J. P. Custer, Jr., A. D. Taggart, S. R. Bottum, S. E. Morley, S. Kim, J. R. McBride, J. M. Atkin, J. F. Cahoon, *Nature* **2023**, *614*, 270–274.
[2] T. Hisatomi, K. Domen, *Nat. Catal.* **2019**, *2*, 387–399.
[3] Q. Wang, K. Domen, *Chem. Rev.* **2020**, *120*, 919–985.
[4] C. Jiang, S. J. A. Moniz, A. Wang, T. Zhang, J. Tang, *Chem. Soc. Rev.* **2017**, *46*, 4645–4660.
[5] X. Tao, Y. Zhao, S. Wang, C. Li, R. Li, *Chem. Soc. Rev.* **2022**, *51*, 3561–3608.
[6] S. Fang, M. Rahaman, J. Bharti, E. Reisner, M. Robert, G. A. Ozin, Y. H. Hu, *Nat. Rev. Method. Prime.* **2023**, *3*, 61.
[7] Z. Huang, N. Luo, C. Zhang, F. Wang, *Nat. Rev. Chem.* **2022**, *6*, 197–214.
[8] M. Hesari, X. Mao, P. Chen, *J. Am. Chem. Soc.* **2018**, *140*, 6729–6740.
[9] K. A. Fichthorn, *Chem. Rev.* **2023**, *123*, 4146–4183.
[10] T. Takata, J. Jiang, Y. Sakata, M. Nakabayashi, N. Shibata, V. Nandal, K. Seki, T. Hisatomi, K. Domen, *Nature* **2020**, *581*, 411–414.
[11] Y. Li, H. Zhou, S. Cai, D. Prabhakaran, W. Niu, A. Large, G. Held, R. A. Taylor, X.-P. Wu, S. C. E. Tsang, *Nat. Catal.* **2024**, *7*, 77–88.
[12] F. Sun, Y. Deng, J. Leng, M. Shi, C. Li, S. Jin, R. Li, W. Tian, *J. Am. Chem. Soc.* **2024**, *146*, 31106–31113.
[13] H. G. Yang, C. H. Sun, S. Z. Qiao, J. Zou, G. Liu, S. C. Smith, H. M. Cheng, G. Q. Lu, *Nature* **2008**, *453*, 638–641.
[14] T. Tachikawa, S. Yamashita, T. Majima, *J. Am. Chem. Soc.* **2011**, *133*, 7197–7204.
[15] J. Pan, G. Liu, G. Q. Lu, H. M. Cheng, *Angew. Chem. Int. Ed.* **2011**, *50*, 2133–2137.
[16] S. Yang, B. X. Yang, L. Wu, Y. H. Li, P. Liu, H. Zhao, Y. Y. Yu, X. Q. Gong, H. G. Yang, *Nat. Commun.* **2014**, *5*, 5355.
[17] J. Yu, J. Low, W. Xiao, P. Zhou, M. Jaroniec, *J. Am. Chem. Soc.* **2014**, *136*, 8839–8842.
[18] C. Xu, W. Yang, Z. Ren, D. Dai, Q. Guo, T. K. Minton, X. Yang, *J. Am. Chem. Soc.* **2013**, *135*, 19039–19045.
[19] L. Mu, B. Zeng, X. Tao, Y. Zhao, C. Li, *J. Phys. Chem. Lett.* **2019**, *10*, 1212–1216.
[20] J. Zhang, K. Liu, B. Zhang, J. Zhang, M. Liu, Y. Xu, K. Shi, H. Wang, Z. Zhang, P. Zhou, G. Ma, *J. Am. Chem. Soc.* **2024**, *146*, 4068–4077.
[21] R. Chen, F. Fan, C. Li, *Angew. Chem. Int. Ed.* **2022**, *61*, e202117567.
[22] X. Wu, J. Li, S. Xie, P. Duan, H. Zhang, J. Feng, Q. Zhang, J. Cheng, Y. Wang, *Chem* **2020**, *6*, 3038–3053.
[23] S. Su, I. Siretanu, D. van den Ende, B. Mei, G. Mul, F. Mugele, *J. Am. Chem. Soc.* **2024**, *146*, 2248–2256.
[24] R. Chen, S. Pang, H. An, J. Zhu, S. Ye, Y. Gao, F. Fan, C. Li, *Nat. Energy* **2018**, *3*, 655–663.
[25] R. Chen, Z. Ren, Y. Liang, G. Zhang, T. Dittrich, R. Liu, Y. Liu, Y. Zhao, S. Pang, H. An, C. Ni, P. Zhou, K. Han, F. Fan, C. Li, *Nature* **2022**, *610*, 296–301.
[26] L. Pan, L. Dai, O. J. Burton, L. Chen, V. Andrei, Y. Zhang, D. Ren, J. Cheng, L. Wu, K. Frohna, A. Abfalterer, T. C. Yang, W. Niu, M. Xia, S. Hofmann, P. J. Dyson, E. Reisner, H. Sirringhaus, J. Luo, A. Hagfeldt, M. Grätzel, S. D. Stranks, *Nature* **2024**, *628*, 765–770.
[27] J. Xue, M. Fujitsuka, T. Tachikawa, J. Bao, T. Majima, *J. Am. Chem. Soc.* **2024**, *146*, 8787–8799.
[28] J. Zhu, S. Pang, T. Dittrich, Y. Gao, W. Nie, J. Cui, R. Chen, H. An, F. Fan, C. Li, *Nano Lett.* **2017**, *17*, 6735–6741.
[29] Y. Zhang, Y. Liu, T. Zhang, X. Gong, Z. Wang, Y. Liu, P. Wang, H. Cheng, Y. Dai, B. Huang, Z. Zheng, *Nano Lett.* **2023**, *23*, 1244–1251.
[30] P. Zhang, T. Ochi, M. Fujitsuka, Y. Kobori, T. Majima, T. Tachikawa, *Angew. Chem. Int. Ed.* **2017**, *56*, 5299–5303.
[31] D. Wu, L. Hu, X. Liu, T. Liu, X. Zhu, Q. Luo, H. Zhang, L. Cao, J. Yang, Z. Jiang, T. Yao, *Nat. Commun.* **2025**, *16*, 726.

[32] G. F. Smoot, M. V. Gorenstein, R. A. Muller, *Phys. Rev. Lett.* **1977**, *39*, 898–901.
[33] S. Su, I. Siretanu, D. van den Ende, B. Mei, G. Mul, F. Mugele, *Adv. Mater.* **2021**, *33*, 2106229.
[34] Y. Chen, C. Xu, S. Li, J. An, L. Li, B. Tang, *J. Am. Chem. Soc.* **2024**, *146*, 31456–31463.
[35] Y. Kozuka, Y. Hikita, T. Susaki, H. Y. Hwang, *Phys. Rev. B* **2007**, *76*, 085129.
[36] L. D. MARKS, *Surf. Sci.* **1985**, *150*, 358–366.
[37] G. Wulff, *Z. Kristallogr. Cryst. Mater.* **1901**, *34*, 449–530.
[38] G. D. Barmparis, Z. Lodziana, N. Lopez, I. N. Remediakis, *Beilstein J. Nanotechnol.* **2015**, *6*, 361–368.
[39] H. X. Lin, Z. C. Lei, Z. Y. Jiang, C. P. Hou, D. Y. Liu, M. M. Xu, Z. Q. Tian, Z. X. Xie, *J. Am. Chem. Soc.* **2013**, *135*, 9311–9314.
[40] M. J. Kim, S. Alvarez, Z. Chen, K. A. Fichthorn, B. J. Wiley, *J. Am. Chem. Soc.* **2018**, *140*, 14740–14746.
[41] a. M. F. D. R. C. Snyder, *Ind. Eng. Chem. Res.* **2008**, *47*, 9812–9833.
[42] J. Zhang, H. Li, Q. Kuang, Z. Xie, *Acc. Chem. Res.* **2018**, *51*, 2880–2887.
[43] F. Lai, Y. Chen, H. Guo, *Phys. Chem. Chem. Phys.* **2019**, *21*, 16486–16496.
[44] J. Jiao, G. Lai, S. Qin, C. Fang, X. Xu, Y. Jiang, C. Ouyang, J. Zheng, *Acta Mater.* **2022**, *238*, 118229.
[45] L. Liu, A. Corma, *Nat. Rev. Chem.* **2021**, *5*, 256–276.
[46] G. Liu, J. C. Yu, G. Q. Lu, H. M. Cheng, *Chem. Commun.* **2011**, *47*, 6763.
[47] S. Wang, G. Liu, L. Wang, *Chem. Rev.* **2019**, *119*, 5192–5247.
[48] G. Liu, H. G. Yang, J. Pan, Y. Q. Yang, G. Q. Lu, H. M. Cheng, *Chem. Rev.* **2014**, *114*, 9559–9612.
[49] Y. Zhang, X. Wu, Z. H. Wang, Y. Peng, Y. Liu, S. Yang, C. Sun, X. Xu, X. Zhang, J. Kang, S. H. Wei, P. F. Liu, S. Dai, H. G. Yang, *J. Am. Chem. Soc.* **2024**, *146*, 6618–6627.
[50] Y. Zhang, Z.-H. Wang, W. Li, P. C. Ding, M. M. Wang, Y. Y. Tang, H. Y. Lin, Y. Peng, M. Y. Wang, Z. Zheng, S. Yang, S. Dai, X. Zhang, P. F. Liu, H. G. Yang, *Angew. Chem. Int. Ed.* **2025**, e202508114.
[51] H. Huang, J. Wang, Y. Liu, M. Zhao, N. Zhang, Y. Hu, F. Fan, J. Feng, Z. Li, Z. Zou, *Nat. Mater.* **2024**, *23*, 383–390.
[52] L. Lin, Z. Lin, J. Zhang, X. Cai, W. Lin, Z. Yu, X. Wang, *Nat. Catal.* **2020**, *3*, 649–655.
[53] F. Qin, Y. Kang, X. San, Y.-L. Tang, J. Li, X. Zhang, K. Zhang, G. Liu, *J. Am. Chem. Soc.* **2025**, *147*, 726–735.
[54] S. Wang, P. Chen, J. H. Yun, Y. Hu, L. Wang, *Angew. Chem. Int. Ed.* **2017**, *56*, 8500–8504.
[55] L. Dong, H. Shi, K. Cheng, Q. Wang, W. Weng, W. Han, *Nano Res.* **2014**, *7*, 1311–1318.
[56] L. Han, Y. Wu, K. Fang, S. Sweeney, U. K. Roesner, M. Parrish, K. Patel, T. Walter, J. Piermattei, A. Trimboli, J. Lefler, C. D. Timmers, X. Z. Yu, V. X. Jin, M. T. Zimmermann, A. J. Mathison, R. Urrutia, M. C. Ostrowski, G. Leone, *Nat. Commun.* **2023**, *14*, 1.
[57] Q. Wang, G. Zhang, W. Xing, Z. Pan, D. Zheng, S. Wang, Y. Hou, X. Wang, *Angew. Chem. Int. Ed.* **2023**, *62*, e202307930.
[58] X. Chu, S. Liu, B.-B. Luan, Y. Zhang, Y. Xi, L.-H. Shao, F.-M. Zhang, Y.-Q. Lan, *Angew. Chem. Int. Ed.* **2025**, *64*, e202422940.
[59] M. Liu, Z. Lv, Y. Peng, Y. Kou, T. Zhao, H. Yu, J. Jia, L. Gao, C. Shang, F. Zhang, D. Zhao, X. Li, *Angew. Chem. Int. Ed.* **2025**, *64*, e202423939.
[60] H. Nishiyama, T. Yamada, M. Nakabayashi, Y. Maehara, M. Yamaguchi, Y. Kuromiya, Y. Nagatsuma, H. Tokudome, S. Akiyama, T. Watanabe, R. Narushima, S. Okunaka, N. Shibata, T. Takata, T. Hisatomi, K. Domen, *Nature* **2021**, *598*, 304–307.
[61] W. Deng, H. Lei, X. Zhang, F. Sheng, J. Shi, X. Zhang, X. Liu, S. Grigorian, X. Zhang, J. Jie, *Adv. Mater.* **2022**, *34*, 2109818.
[62] Y. Shang, L. Guo, *Adv. Sci.* **2015**, *2*, 1500140.
[63] S. Chen, D. Huang, P. Xu, X. Gong, W. Xue, L. Lei, R. Deng, J. Li, Z. Li, *ACS Catal.* **2020**, *10*, 1024–1059.
[64] Z. Wang, T. Hisatomi, R. Li, K. Sayama, G. Liu, K. Domen, C. Li, L. Wang, *Joule* **2021**, *5*, 344–359.
[65] T. Takata, L. Lin, T. Hisatomi, K. Domen, *Adv. Mater.* **2024**, *36*, 2406848.
[66] B. P. Labat F, C. Adamo, *J. Chem. Theory Comput.* **2008**, *4*, 341–352.
[67] M. Jacobs, J. Krumland, C. Cocchi, *ACS Appl. Nano Mater.* **2022**, *5*, 5187–5195.
[68] Y. Bi, S. Ouyang, N. Umezawa, J. Cao, J. Ye, *J. Am. Chem. Soc.* **2011**, *133*, 6490–6492.
[69] J. Tao, T. Luttrell, M. Batzill, *Nat. Chem.* **2011**, *3*, 296–300.
[70] C. Shi, S. Ye, X. Wang, F. Meng, J. Liu, T. Yang, W. Zhang, J. Wei, N. Ta, G. Q. M. Lu, M. Hu, J. Liu, *Adv. Sci.* **2021**, *8*, 2001987.
[71] Z. Bian, T. Tachikawa, P. Zhang, M. Fujitsuka, T. Majima, *J. Am. Chem. Soc.* **2014**, *136*, 458–465.
[72] C. S. Ponseca, Jr., P. Chabera, J. Uhlig, P. Persson, V. Sundstrom, *Chem. Rev.* **2017**, *117*, 10940–11024.
[73] R. Chen, C. Ni, J. Zhu, F. Fan, C. Li, *Nat. Protoc.* **2024**, *19*, 2250–2282.
[74] X. Mao, P. Chen, *Nat. Mater.* **2022**, *21*, 331–337.
[75] S. Sun, M. Yang, J. Cui, S. Liang, *Adv. Funct. Mater.* **2022**, *32*, 2106982.
[76] G. Zeng, K. K. Li, H. G. Yang, Y. H. Zhang, *Vib. Spectrosc.* **2013**, *68*, 279–284.
[77] M. Li, S. Yu, H. Huang, X. Li, Y. Feng, C. Wang, Y. Wang, T. Ma, L. Guo, Y. Zhang, *Angew. Chem. Int. Ed.* **2019**, *58*, 9517–9521.
[78] K. Zhang, Y. Lu, Q. Zou, J. Jin, Y. Cho, Y. Wang, Y. Zhang, J. H. Park, *ACS Energy Lett.* **2021**, *6*, 4071–4078.
[79] X. Chen, C. Zhen, J. Li, J. Qiu, N. Li, N. Jia, G. Liu, *Adv. Funct. Mater.* **2024**, *34*, 2409566.
[80] W. Shao, X. Xu, W. Zheng, Z. Wang, Q. Pan, X. Liu, W. Tao, F. Liu, C. Zhu, P.-H. Tan, H. Zhu, H. Song, Y. Han, T. Sun, J. Zhao, X. Li, Y. Zhu, *Joule* **2024**, *8*, 141–156.
[81] C. Ma, F. T. Eickemeyer, S. H. Lee, D. H. Kang, S. J. Kwon, M. Grätzel, N. G. Park, *Science* **2023**, *379*, 173–178.
[82] D. Dai, X. Liang, B. Zhang, Y. Wang, Q. Wu, X. Bao, Z. Wang, Z. Zheng, H. Cheng, Y. Dai, B. Huang, P. Wang, *Adv. Sci.* **2022**, *9*, 2105299.
[83] R. Chen, F. Fan, T. Dittrich, C. Li, *Chem. Soc. Rev.* **2018**, *47*, 8238–8262.
[84] Z. Luo, X. Ye, S. Zhang, S. Xue, C. Yang, Y. Hou, W. Xing, R. Yu, J. Sun, Z. Yu, X. Wang, *Nat. Commun.* **2022**, *13*, 2230.
[85] C. Foo, Y. Li, K. Lebedev, T. Chen, S. Day, C. Tang, S. C. E. Tsang, *Nat. Commun.* **2021**, *12*, 661.
[86] T. Liu, X. Zhou, M. Dupuis, C. Li, *Phys. Chem. Chem. Phys.* **2015**, *17*, 23503–23510.
[87] D. Li, Y. Liu, W. Shi, C. Shao, S. Wang, C. Ding, T. Liu, F. Fan, J. Shi, C. Li, *ACS Energy Lett.* **2019**, *4*, 825–831.
[88] G. Wan, L. Yin, X. Chen, X. Xu, J. Huang, C. Zhen, H. Zhu, B. Huang, W. Hu, Z. Ren, H. Tian, L. Wang, G. Liu, H. M. Cheng, *J. Am. Chem. Soc.* **2022**, *144*, 20342–20350.
[89] T. L.e Bahers, M. Rérat, P. Sautet, *J. Phys. Chem. C* **2014** *118*, 5997–6008.
[90] J. Ravichandran, W. Siemons, M. L. Scullin, S. Mukerjee, M. Huijben, J. E. Moore, A. Majumdar, R. Ramesh, *Phys. Rev. B* **2011**, *83*, 035101.
[91] R. Lin, J. Wan, Y. Xiong, K. Wu, W. C. Cheong, G. Zhou, D. Wang, Q. Peng, C. Chen, Y. Li, *J. Am. Chem. Soc.* **2018**, *140*, 9078–9082.
[92] C. M. Wolff, P. D. Frischmann, M. Schulze, B. J. Bohn, R. Wein, P. Livadas, M. T. Carlson, F. Jäckel, J. Feldmann, F. Würthner, J. K. Stolarczyk, *Nat. Energy* **2018**, *3*, 862–869.

[93] T. Liu, Z. Pan, K. Kato, J. J. M. Vequizo, R. Yanagi, X. Zheng, W. Yu, A. Yamakata, B. Chen, S. Hu, K. Katayama, C. Chu, *Nat. Commun.* **2022**, *13*, 7783.
[94] H. Yan, H. Lei, X. Qin, J. C. Liu, L. Cai, S. Hu, Z. Xiao, F. Peng, W. W. Wang, Z. Jin, X. Yi, A. Zheng, C. Ma, C. J. Jia, J. Zeng, *Angew. Chem. Int. Ed.* **2024**, *63*, e202411264.
[95] B. Zhang, X. Huang, Y. Zhang, G. Lu, L. Chou, Y. Bi, *Angew. Chem. Int. Ed.* **2020**, *59*, 18990–18995.
[96] H. Wang, F. Wang, S. Zhang, J. Shen, X. Zhu, Y. Cui, P. Li, C. Lin, X. Li, Q. Xiao, W. Luo, *Adv. Mater.* **2024**, *36*, 2400764.
[97] R. Li, F. Zhang, D. Wang, J. Yang, M. Li, J. Zhu, X. Zhou, H. Han, C. Li, *Nat. Commun.* **2013**, *4*, 1432.
[98] S. Selcuk, A. Selloni, *Nat. Mater.* **2016**, *15*, 1107–1112.
[99] G. Zhou, B. Lei, F. Dong, *ACS Catal.* **2024**, *14*, 4791–4798.
[100] S. Selim, E. Pastor, M. Garcia-Tecedor, M. R. Morris, L. Francas, M. Sachs, B. Moss, S. Corby, C. A. Mesa, S. Gimenez, A. Kafizas, A. A. Bakulin, J. R. Durrant, *J. Am. Chem. Soc.* **2019**, *141*, 18791–18798.
[101] S. M. H. Hejazi, M. Shahrezaei, P. Błoński, M. Allieta, P. M. Sheverdyaeva, P. Moras, Z. Bad'ura, S. Kalytchuk, E. Mohammadi, R. Zbořil, Š. Kment, M. Otyepka, A. Naldoni, P. Fornasiero, *Chem Catal.* **2022**, *2*, 1177–1190.
[102] D. Wang, T. Sheng, J. Chen, H.-F. Wang, P. Hu, *Nat. Catal.* **2018**, *1*, 291–299.
[103] P. You, D. Chen, X. Liu, C. Zhang, A. Selloni, S. Meng, *Nat. Mater.* **2024**, *23*, 1100–1106.
[104] H. Zhang, P. Sun, X. Fei, X. Wu, Z. Huang, W. Zhong, Q. Gong, Y. Zheng, Q. Zhang, S. Xie, G. Fu, Y. Wang, *Nat. Commun.* **2024**, *15*, 4453.
[105] H. Zhou, M. Wang, F. Kong, Z. Chen, Z. Dou, F. Wang, *J. Am. Chem. Soc.* **2022**, *144*, 21224–21231.
[106] B. Li, F. Tong, M. Lv, Z. Wang, Y. Liu, P. Wang, H. Cheng, Y. Dai, Z. Zheng, B. Huang, *ACS Catal.* **2022**, *12*, 9114–9124.

Manuscript received: May 28, 2025
Revised manuscript received: June 26, 2025
Accepted manuscript online: July 15, 2025
Version of record online: July 24, 2025